

6.10 High-Valent Pd Coordination Compounds

Sagnik Chakrabarti*, Soumalya Sinha*, and Liviu M. Mirica, Department of Chemistry, University of Illinois at Urbana-Champaign, Urbana, IL, United States

© 2021 Elsevier Ltd. All rights reserved.

6.10.1	Introduction	375
6.10.2	Pd^{III} Complexes	376
6.10.2.1	Mononuclear Pd ^{III} Complexes	376
6.10.2.1.1	Pd ^{III} complexes stabilized by tetradentate RN ₄ ligands	376
6.10.2.1.2	Pd ^{III} complexes stabilized by tetradentate RN ₃ CH ligands	378
6.10.2.1.3	Pd ^{III} complexes stabilized by [9]aneS ₃ and [18]aneS ₆ ligands	378
6.10.2.1.4	Pd ^{III} complexes stabilized by terpyridyl ligands	379
6.10.2.2	Dinuclear Pd^{III} Complexes	379
6.10.2.2.1	Mixed-valent Pd ^{II} –Pd ^{III} complexes	379
6.10.2.2.2	Pd ^{III} complexes featuring a Pd ^{III} –Pd ^{III} bond	380
6.10.2.2.3	Molecular 1D chains bearing Pd ^{III} –Pd ^{III} bonds	382
6.10.2.2.4	Pd ^{III} complexes featuring no Pd ^{III} –Pd ^{III} bonds	383
6.10.3	Pd^{IV} Complexes	384
6.10.3.1	Pd ^{IV} Complexes Stabilized by Bidentate Ligands	385
6.10.3.1.1	Pd ^{IV} complexes stabilized by bipyridyl and 2-phenylpyridyl ligands	385
6.10.3.1.2	Pd ^{IV} complexes stabilized by terpyridyl ligands	389
6.10.3.2	Pd ^{IV} Complexes Stabilized by Conformationally Flexible Ligands	391
6.10.3.2.1	Pd ^{IV} complexes stabilized by the Me ₃ tacn ligand	391
6.10.3.2.2	Pd ^{IV} complexes stabilized by pyridinophane ligands	392
6.10.3.3	Pd ^{IV} Complexes Stabilized by Tridentate Facial Chelating Ligands	393
6.10.3.3.1	Pd ^{IV} complexes stabilized by tris-(pyrazolylborate) (Tp) ligands	393
6.10.3.3.2	Pd ^{IV} complexes stabilized NNO or NCO donors based on diaryl ketones	396
6.10.3.3.3	Pd ^{IV} complexes stabilized by di(pyridin-2-yl)methane ligands	397
6.10.3.3.4	Pd ^{IV} complexes stabilized by the Kläui ligand	397
6.10.3.4	Pd ^{IV} Complexes Stabilized by Tridentate Planar Ligands	398
6.10.3.4.1	Pd ^{IV} complexes stabilized by pincer ligands	398
6.10.3.4.2	Pd ^{IV} complexes stabilized by terpyridyl ligands	400
6.10.3.5	Pd ^{IV} Complexes Stabilized by Other Ligand Systems	401
6.10.4	Summary and Outlook	404
References		404

Key Terms

Pd(III) complexes Coordination compounds containing Pd center(s) in the +3 oxidation state

Pd(IV) complexes Coordination compounds containing Pd center(s) in the +4 oxidation state

6.10.1 Introduction

Palladium holds a privileged position in inorganic and organometallic chemistry. It is virtually synonymous with transition metal-catalyzed cross-coupling chemistry, a strategy that allows the construction of carbon-carbon bonds with relative ease. This was recognized in 2010, when Heck, Negishi, and Suzuki were awarded the Nobel Prize in Chemistry for developing “Palladium Catalyzed Cross-Couplings in Organic Synthesis.” The success can be, in large part, attributed to the extensive mechanistic investigations into the elementary steps of these catalytic cycles, nearly all of which feature Pd⁰ and Pd^{II} oxidation states and thus can be called ‘low-valent’ palladium chemistry.¹ Careful investigation revealed the interplay between the steric and electronic effects of the ligands, which helped fine-tune the reactivity.

However, low-valent palladium chemistry is not suitable for certain transformations such as oxidative carbon-heteroatom bond formations and is susceptible to decomposition pathways such as β-hydride elimination. In the past couple of decades, the field of

*These authors contributed equally.

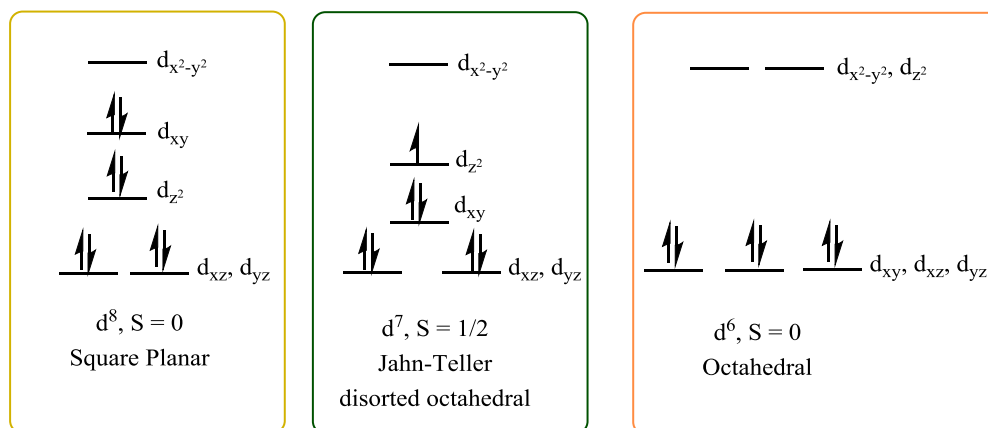


Fig. 1 Pictorial representation of d electronic configuration of a Pd center in the +2, +3, and +4 oxidation states.

'high-valent' Pd catalysis has received a lot of attention from several research groups, and Pd^{III} and Pd^{IV} intermediates have been invoked in the various proposed catalytic cycles. In the 1980s and 1990s, several studies reported well-defined organometallic Pd^{III} and Pd^{IV} coordination complexes, and the interest has grown extensively in developing this high-valent chemistry as a complement to the traditional low-valent chemistry.^{2–4}

To understand the reactivity of high-valent Pd centers, it is worthwhile to look at their electronic structure in order to understand the nature of the ligand field required to stabilize such complexes. Pd^{III} centers, with a d⁷ configuration, are expected to have a distorted octahedral geometry with the unpaired electron located in the d_{z²} orbital (**Fig. 1**).^{3,5} Studies have shown the unpaired electron is usually metal-centered, though complexes with highly covalent bonds exhibit a significant contribution of the ligand orbitals to the singly-occupied molecular orbital (SOMO). The existence of a metal-based unpaired electron also means that Pd^{III} complexes are prone to form dinuclear complexes with a Pd–Pd bond, or with a bridging halide.

Pd^{IV}, on the other hand, almost exclusively forms symmetric octahedral complexes. They are low spin, diamagnetic, and are stabilized by strong σ -donors. They are not as stable as their Pt^{IV} congeners, as expected from the decrease in ligand field stabilization energy in going from 5d to 4d transition metals. Hence, they are often prone to thermal decomposition via reductive elimination. The usual strategy of generating Pd^{IV} complexes has been the oxidative addition to Pd^{II} species of alkyl/aryl halides, halogens, or the use of strong oxidants like peroxosulfates, several other peroxy compounds, hypervalent iodine reagents, N-halosuccinimides, etc. However, recent examples have also emerged where oxidation of Pd^{II} precursors using mild oxidants such as molecular oxygen has been successful.

This chapter describes examples of isolated high-valent palladium complexes reported since 2003 that have been fully characterized by X-ray diffraction or using various spectroscopic techniques to unequivocally establish the oxidation state of the Pd centers. Several reviews have highlighted the importance of Pd^{III} and Pd^{IV} in the context of organic reactions, and these are beyond the purview of the current discussion.^{6–8} Importantly, the last few decades have seen a significant growth of the field of high-valent palladium chemistry.

6.10.2 Pd^{III} Complexes

6.10.2.1 Mononuclear Pd^{III} Complexes

6.10.2.1.1 Pd^{III} complexes stabilized by tetradentate RN4 ligands

A series of mononuclear Pd^{II} and Pd^{III} complexes bearing tetradentate *N,N'*-dialkyl-2,11-diaza[3.3](2,6)pyridinophane (RN4), where alkyl group (R) = ^tBu, Me, or ⁱPr, was investigated by Mirica and coworkers (**Fig. 2**).^{9–11} The RN4 ligands were shown to lower

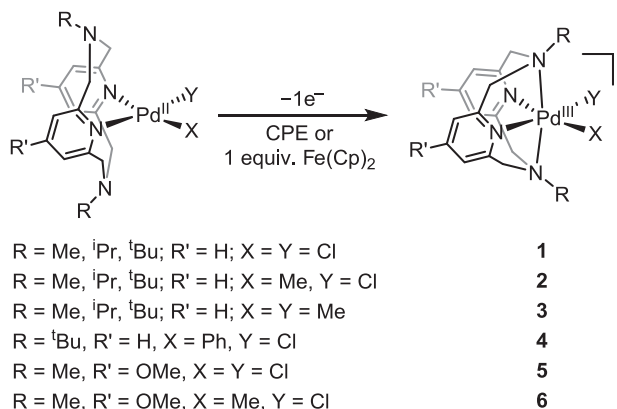


Fig. 2 Synthesis of mononuclear Pd^{III} complexes stabilized by RN4 ligands.

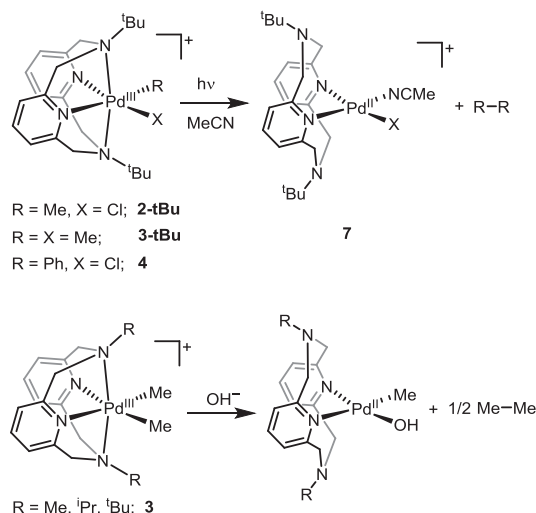


Fig. 3 Selected reactivity of mononuclear Pd^{III} complexes bearing the ^tBuN4 ligand.

the Pd^{II/III} redox potential and offered an electrochemical synthesis approach to oxidize the (RN4)Pd^{II} precursors to the corresponding Pd^{III} complexes (1–6). Alternatively, chemical oxidation of those Pd^{II} complexes using mild chemical oxidants, e.g., ferrocenium or O₂, also yielded the corresponding Pd^{III} complexes such as 3. The early studies were mainly based on the ^tBuN4 ligand, and the steric effects of the ^tBuN4 ligand supported the stabilizing factor for Pd^{III} complexes over Pd^{II} or Pd^{IV} complexes. For example, the electrochemical oxidation of the green Pd^{III} complex 5-**tBu** at low temperature yielded a red species tentatively assigned to the corresponding Pd^{IV} complex, which reverts back to the Pd^{III} complex 5-**tBu** within 1 h at room temperature.¹² Interestingly, these Pd^{III} complexes exhibit both light-induced or exogenous ligand-promoted C–C bond formation reactivity (Fig. 3).¹⁰

X-ray crystallographic data revealed Jahn-Teller distorted octahedral geometries at the d⁷ Pd^{III} metal center, with elongated axial Pd–N_{amine} bonds (Pd–N_{axial}, 2.41–2.48 Å) compared to the equatorial Pd–N_{pyridyl} bonds for these mononuclear Pd^{III} complexes.¹² The steric effect of the axial N-substituents also influences the Pd–N_{axial} bond lengths, where bulkier N-substituents show longer Pd–N_{axial} bonds in the order, ^tBuN4 > ⁱPrN4 > MeN4.¹³

Furthermore, the N-alkyl substituents were shown to tune the redox properties of the Pd^{II}/Pd^{III} center. To explore the steric effect along with the electronic effect of the axial N-substituent on the metal center, the electron-rich Me(*p*-OMe)N4 ligand and its corresponding Pd^{II} and Pd^{III} complexes were synthesized.¹¹ The cyclic voltammogram (CV) recorded for 1-Me in non-aqueous electrolyte showed that the redox potentials for the Pd^{II/III} and Pd^{III/IV} oxidation events are similar to the identical redox events for 5, but significantly lower, ≤ 180 mV for E_{pa}^{II/III} and ≤ 300 mV for E_{pa}^{III/IV}, than those of 1-**tBu** under the same electrochemical conditions. Such a trend is also observed for the (RN4)Pd^{II}MeCl complexes.¹¹ Together, these electrochemical data suggest that the substituents on the pyridyl backbone barely affect the redox properties of the Pd center, while the steric properties of the N-substituents are dominating, as exemplified by the experimentally determined axial Pd–N_{amine} bond lengths (Fig. 4). In addition, the same group reported in 2020 that the use of electron withdrawing N-tosyl substituents on the RN4 ligand led to the formation of (RN4)Pd^{III} complexes that were significantly destabilized such that they could only be observed in situ.¹⁴

In 2014, additional electrochemical studies, including CV, differential pulse voltammetry, and CV simulations reported by the same group revealed that the ^tBuN4 ligand adopts different coordination modes, such as bidentate (κ²), tridentate (κ³), or tetradentate (κ⁴) ligation, and this conformational flexibility can reduce the potential barrier for the oxidation of the Pd^{II} precursors.¹⁵ These oxidation processes are governed by the minor conformations in which either one or both of the two axial amine N donors are coordinated to the Pd^{II} center. Additionally, the observed conformationally-dependent redox behavior can be tuned by varying the temperature, with the most stable isomer dominating the electrochemical behavior at low temperatures, whereas rapid conformational changes occurred at room temperature. Overall, the authors concluded the coordination to the Pd center of each axial amine donor of the ^tBuN4 ligand leads to a lowering of the Pd^{II}/Pd^{III} oxidation potential by ~0.6 V. In the same study, a rare dicationic Pd^{III} complex [(^tBuN4)Pd^{III}Me(MeCN)]²⁺, 8, was structurally characterized and it exhibited shorter axial Pd–N_{amine} bonds

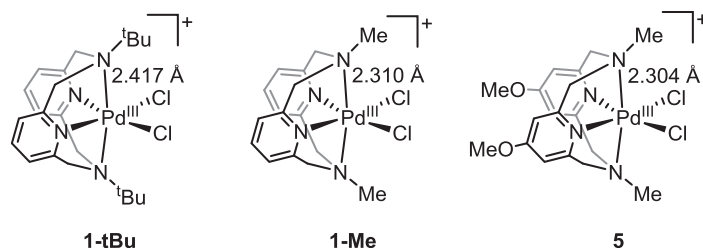


Fig. 4 Comparison of the average axial Pd–N_{amine} bond lengths for three similar Pd^{III} complexes stabilized by RN4 ligands.

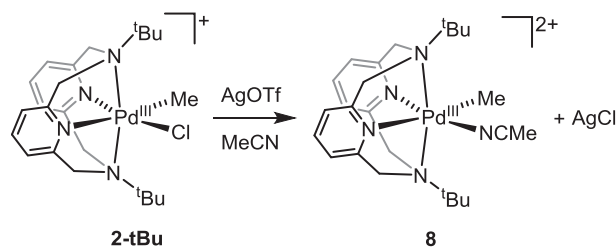


Fig. 5 Synthesis of a mononuclear $[(^t\text{BuN4})\text{Pd}^{\text{III}}\text{Me}(\text{MeCN})]^{2+}$ complex.

that those of the analogous monocationic Pd^{III} complexes, as expected given a stronger electrostatic attraction between the Pd center and the amine N donors (Fig. 5).

The $(\text{RN4})\text{Pd}^{\text{III}}$ complexes were also investigated by EPR spectroscopy, and they usually exhibit either axial and rhombic patterns with average g values of 2.11–2.14, which are attributed to a d_{z^2} ground state for the Pd^{III} center, along with axial ^{14}N superhyperfine coupling constants, supporting the interaction between Pd^{III} center and the axial N donors.^{9,11} Indeed, DFT calculations of the Pd^{III} complexes revealed that the unpaired electron is mainly localized on the metal-based d_{z^2} atomic orbital. Time-dependent DFT studies support the assignment of the three absorption bands at 723–741, 554–594, and 353–386 nm, for the above mentioned $(^t\text{BuN4})\text{Pd}^{\text{III}}$ complexes, as LMCT transitions, a combination of d-d and LMCT transitions, and LMCT transitions, respectively.⁹

6.10.2.1.2 Pd^{III} complexes stabilized by tetradentate RN3CH ligands

In 2019, the Mirica group introduced a modified pyridinophane ligand by replacing one of the pyridyl groups with a *para*-functionalized phenyl donor group, $^t\text{Bu}(p\text{-R})\text{N3CH}$ ($\text{R} = \text{H}, \text{Me}, \text{OMe}, \text{CN}$) that stabilizes both Pd^{III} and Pd^{IV} complexes.¹⁶ Such a $^t\text{Bu}(p\text{-R})\text{N3CH}$ ligand resembles the NCN type pincer ligands,¹⁷ yet it also includes an additional pyridine donor group. Interestingly, the Pd^{II} complex **9** does not undergo $\text{C}_{\text{aryl}}\text{-H}$ bond activation, even upon heating or the addition of excess acetate. However, under the Kharasch radical addition conditions in the presence of CCl_3Br and methyl methacrylate (MMA), C–H bond activation has been observed to generate Pd^{III} complexes such as **10**, which were isolated and characterized (Fig. 6). Furthermore, additional $(^t\text{Bu}(p\text{-Me})\text{N3C})\text{Pd}^{\text{III}}$ complexes **12** and **13** were also obtained by reacting to their Pd^{II} analogs with PhICl_2 , followed by halide abstraction with thallium salts. Additionally, $1e^-$ oxidation of such Pd^{III} complex yielded Pd^{IV} complexes, including a rare tricationic Pd^{IV} complex **14** (*vide infra*).

X-ray crystallography of **12** confirmed a distorted octahedral geometry where a single Cl and a single MeCN ligand occupy the equatorial positions, *trans* to the pyridyl N atom and the phenyl C atom, respectively. It is worth mentioning that the $\text{Pd}^{\text{III}}\text{-C}_{\text{aryl}}$ bond (1.945–1.989 Å) has been formed upon oxidation of the analogous Pd^{II} complex bearing a non-coordinating C–H bond. Moreover, the EPR spectra of these Pd^{III} complexes exhibited rhombic, anisotropic signals, confirming the presence of a d^7 Pd^{III} center with a d_{z^2} ground state. Overall, these results show that the RN3CH ligands are capable of stabilizing a range of high-valent Pd complexes.

6.10.2.1.3 Pd^{III} complexes stabilized by [9]aneS₃ and [18]aneS₆ ligands

In 2012, the air-stable mononuclear Pd^{III} complexes supported by the macrocyclic ligands [9]aneS₃ and [18]aneS₆, **15**, and **16**, respectively, were reported by Schröder and coworkers (Fig. 7).¹⁸ These complexes were synthesized by oxidizing their Pd^{II}

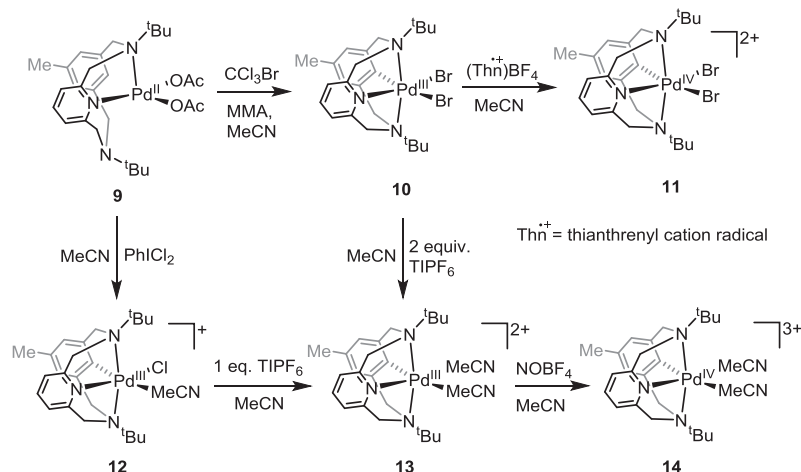


Fig. 6 Syntheses of Pd^{III} and Pd^{IV} complexes bearing the $^t\text{Bu}(p\text{-Me})\text{N3C}$ ligand.

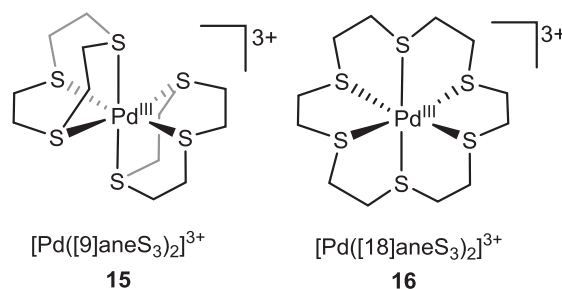


Fig. 7 Mononuclear Pd^{III} complexes stabilized by the [9]aneS3 (left) and [18]aneS6 (right) ligands.

derivatives either by performing controlled potential electrolysis in 0.2 M ⁿBu₄PF₆ MeCN or through a chemical oxidation process using 70% HClO₄. X-ray crystallography data revealed that **15** and **16** are in Jahn-Teller distorted octahedral geometry, as expected for a d⁷ Pd^{III} center, with comparatively shorter axial Pd–S distances (2.5356 Å) and elongated equatorial Pd–S bond lengths by about 0.05–0.06 Å than that of their Pd^{II} derivatives, [Pd([9]aneS₃)₂]²⁺ and [Pd([18]aneS₆)₂]²⁺, respectively. Multifrequency EPR studies for these Pd^{III} complexes as fluid (233K) or frozen (77 K) revealed similar g-values for g_{xx} (2.048) and g_{yy} (2.046 and 2.036 for **15** and **16**, respectively) that corresponds to the equatorial plane contributions, and lower g_{zz} values, 2.004 (for **15**) and 1.998 (for **16**) for the axial contribution. DFT calculations also support such interpretation with the prediction that the dominant metal contribution of the singly occupied molecular orbital is due to the Pd 4d_{z²} orbital.

6.10.2.1.4 Pd^{III} complexes stabilized by terpyridyl ligands

A monomeric Pd^{III} complex **18** stabilized by the terpyridine (terpy) ligand was synthesized by treating its Pd^{II} analog **17** using one equivalent of terpy ligand, followed by one equivalent of Selectfluor (**Fig. 8**).¹⁹ A deep red color solution in MeCN was obtained, and red needles of the Pd^{III}(terpy) complex **18** were finally collected upon crystallization. X-ray crystallography data confirmed the Jahn-Teller distorted octahedral geometry and the EPR spectrum collected at 77 K also supported the d⁷ Pd configuration (g_{ave} = 2.09) with the unpaired electron residing at d_{z²} orbital, rather than a ligand-centered radical. Interestingly, the solid Pd^{III} complex was stable for months at ambient conditions and capable of performing a fluorination reaction in the presence of Selectfluor.

6.10.2.2 Dinuclear Pd^{III} Complexes

6.10.2.2.1 Mixed-valent Pd^{II}–Pd^{III} complexes

In 2007, dinuclear mixed-valent Pd^{II}Pd^{III} complexes **20a–20c** stabilized with di-*p*-anisylformamidinate ligands were synthesized by one-electron chemical oxidation of their corresponding Pd^{II}Pd^{II} precursor (**Fig. 9**).²⁰ The Pd–Pd distances of ~2.60 Å in the mixed

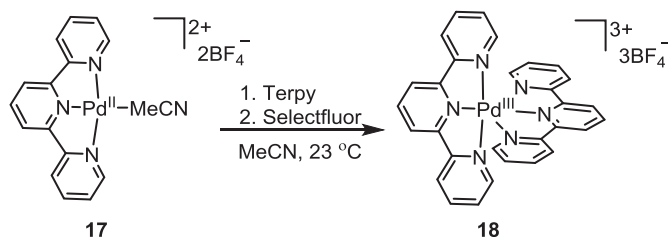


Fig. 8 Synthesis of mononuclear Pd^{III} complexes stabilized by the terpyridine ligand.

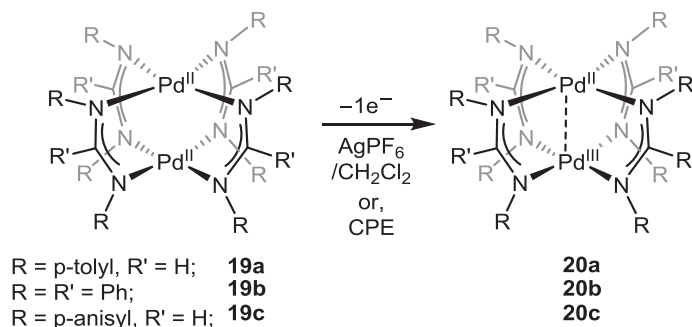


Fig. 9 Synthesis of mixed-valent Pd^{II}–Pd^{III} complexes.

valent Pd^{II}Pd^{III} complexes are 0.05 Å shorter than those of their dinuclear Pd^{II} precursors, as expected for the increase in the Pd–Pd bond order. Detailed EPR studies carried out for such Pd^{II}Pd^{III} complexes confirmed that the unpaired electron resides mostly on Pd-based molecular orbitals, by exhibiting a rhombic signal with different g values by high-field EPR and a broad isotropic signal in the X-band EPR spectrum, as similarly observed for the previously reported di-*p*-tolylformamidinate complexes.^{21,22}

6.10.2.2.2 Pd^{III} complexes featuring a Pd^{III}–Pd^{III} bond

6.10.2.2.2.1 Pd^{III} complexes stabilized by orthometalated phosphine ligands

In 2006, Cotton et al. reported the first organometallic dinuclear Pd^{III} complexes, **22a–22c** stabilized by two orthometalated phosphine ligands, two bridging carboxylate groups, and a Cl[−] ion ligated to each Pd center (Fig. 10).²³ X-ray crystallography data revealed a short Pd^{III}–Pd^{III} bond distance of 2.524–2.543 Å that was further supported by DFT calculations, which also showed that the axial chloride coordination lengthens the Pd–Pd single bond. Ubeda, Fernández, and co-workers also reported similar organometallic dinuclear Pd^{III} complexes and their reactivity toward the diborylation of vinylarenes and aliphatic 1-alkenes were investigated under mild reaction conditions.^{24,25} These dinuclear Pd^{III} complexes showed a high turnover with high chemoselectivity for diverse types of 1,2-diboronate esters production.

In 2016, Ubeda and co-workers used the identical two orthometalated phosphine ligands along with two pyrazolates to stabilize dinuclear Pd^{III}–Pd^{III} complexes where two chlorides reside in the axial positions (Fig. 11).²⁶ X-ray crystallography revealed significantly short Pd–Pd bond distances of 2.505 and 2.507 Å for **24a** and **24b**, respectively, compared to the other known dinuclear Pd^{III} complexes stabilized with “paddlewheel” orthometalated phosphine ligands. The dihedral angle value observed for the two Pd–N–N–Pd fragments was 88.04° (**24a**) and 85.92° (**24b**), similar to their Pd^{II} derivatives. Furthermore, the axial chlorides reside between two pyrazolate rings with the Pd–Pd–Cl angle of 163.4° (**24a**) and 162.3° (**24b**).

6.10.2.2.2.2 Pd^{III} complexes stabilized by benzo[*h*]quinoline ligands

In 2009, Ritter and co-workers prepared the dinuclear Pd^{II} complex **25** by reacting Pd(OAc)₂ and benzo[*h*]quinoline that can then be rapidly oxidized using PdICl₂ or PdI(OAc)₂ to yield dinuclear Pd^{III} complexes **26a** and **26b** that are stable at temperatures below −30 °C (Fig. 12).^{27,28} X-ray crystal structure of such Pd^{III} dimers showed a Pd–Pd bond distance of 2.57 Å that was further supported by DFT calculations, which revealed a Pd–Pd bonding interaction between the two Pd centers, each having a d⁷ electronic configuration.²⁹ Interestingly, when the Pd^{II} dimer **25** was reacted with a trifluoromethylating agent in the presence of acetic acid, a monomeric Pd^{IV} complex **28** was obtained.³⁰ Later, in 2012, it was described that such an oxidation process from **25** to **28** involves a dinuclear Pd^{III} intermediate that undergoes heterolytic disproportionation to form complex **28**.³¹

While the dinuclear Pd^{III} complexes **26a–b** are stable at low temperatures, they undergo rapid reductive elimination to generate a new C-heteroatom bond in quantitative yields (Fig. 13).²⁸

The reaction mechanism was also investigated by Ritter, Goddard, and co-workers to elucidate whether the dinuclear Pd^{III} complex is directly involved in the reductive elimination process.³² Five different possible intermediate processes from the Pd^{III}

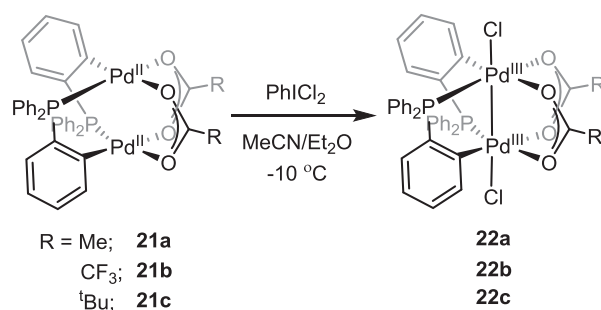


Fig. 10 Syntheses of dinuclear Pd^{III} complexes stabilized by orthometalated phosphine ligands and bridging carboxylate groups.

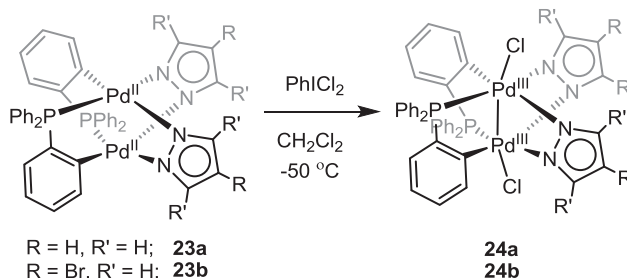


Fig. 11 Syntheses of dinuclear Pd^{III} complexes stabilized by orthometalated phosphine ligands and bridging pyrazolate groups.

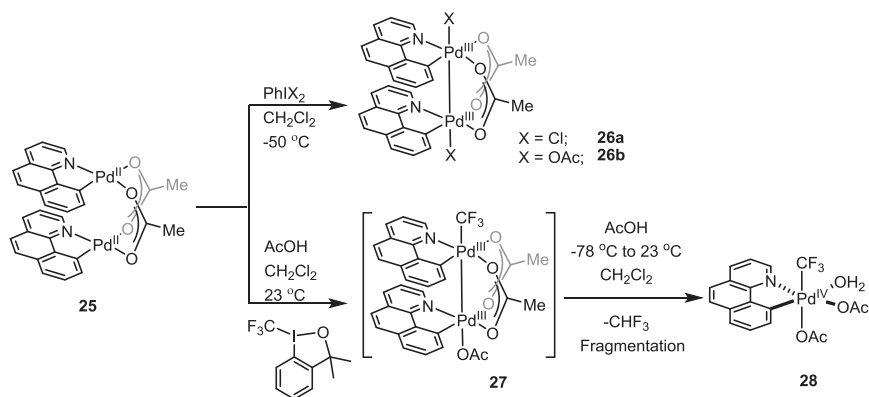


Fig. 12 Syntheses of dinuclear Pd^{III} complexes and a mononuclear Pd^{IV} complex stabilized by the benzo[*h*]quinoline ligand.

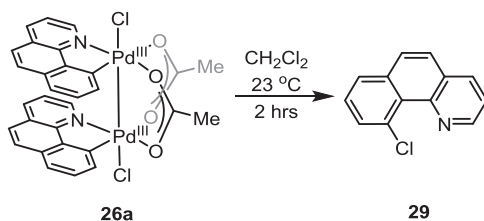


Fig. 13 C-Cl Bond formation reactivity of a dinuclear Pd^{III} complex.

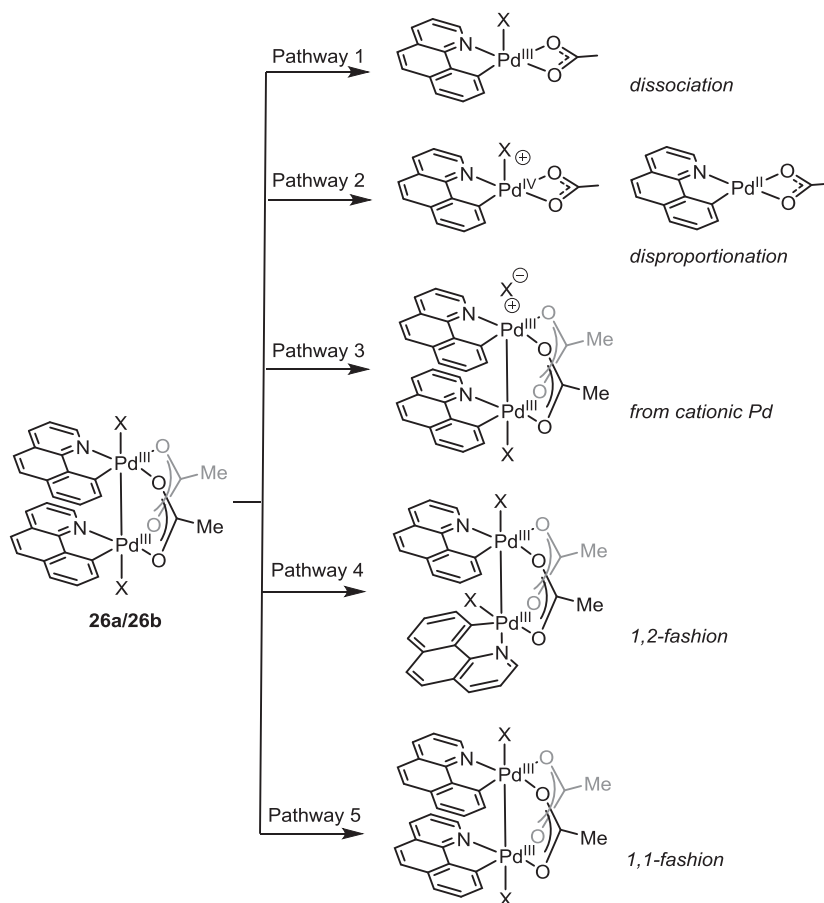


Fig. 14 Aryl-Cl and aryl-OAc bond formation from a dinuclear Pd^{III} complex stabilized by the benzo[*h*]quinoline ligand.³³

dimers **26a-b** were proposed that could be responsible for the reduction elimination step (Fig. 14): (1) dissociation into a mononuclear Pd^{III} complex (Pathway 1), (2) disproportionation into a Pd^{II} and Pd^{IV} species, followed by reductive elimination from the Pd^{IV} complex (Pathway 2), (3) loss of Cl⁻ and subsequent reductive elimination from a cationic Pd^{III} center (Pathway 3), or (4) direct reductive elimination from the neutral Pd^{III} dimer itself either in 1,2 fashion (Pathway 4) or 1,1 fashion (Pathway 5).^{33,34} Pathways 1 and 3 were ruled out based on the kinetic studies, and pathway 2 is most likely not happening as the proposed Pd^{II} and Pd^{IV} species were not observed experimentally. However, computational studies indicated that Pd–Pd bond with bridging acetate is important to facilitate the reductive elimination at a lower energy barrier at room temperature.³² In between pathways 4 and 5, pathway 4 was eliminated as the occurrence of concerted 4-center (C–Pd–Pd–Cl) is symmetry forbidden, and thus, the pathway 5 has been proposed as the most viable, involving a bimetallic reductive elimination promoted by synergistic metal-metal cooperation.³⁵

In 2013, Schoenebeck and co-workers synthesized a related dinuclear Pd^{III} complex, **30**, by oxidizing the corresponding Pd^{II} precursor with acetyl hypochlorite, and they observed 54% aryl chloride and 4% aryl acetate formation via reductive elimination (Fig. 15).³⁴ They interpreted such behavior as a “ligand scrambling” at the dinuclear Pd^{III} complex **30** that provides a 1:1 mixture of compounds **26a** and **26b**, which was further confirmed via ¹H NMR spectroscopy.

6.10.2.2.3 Molecular 1D chains bearing Pd^{III}–Pd^{III} bonds

The oxidation of the dinuclear Pd^{II} complexes **25** and **31** stabilized with benzo[*h*]quinolynyl complexes²⁸ using one equivalent of XeF₂ formed the one-dimensional molecular wires **32a-32b** that contain Pd^{III}–Pd^{III} bonds, as reported by Ritter et al. in 2011 (Fig. 16). X-ray crystallography analysis revealed an infinite chain of Pd^{III}–Pd^{III} interactions with Pd^{III}–Pd^{III} bond distances of 2.72 Å, and coordination of the fluoride ions. Dynamic and static light scattering experiments, along with concentration-dependent NIR absorption, also supported these Pd^{III} based molecular wires. Noteworthy, the addition of ⁿBu₄NCl to the Pd^{III}

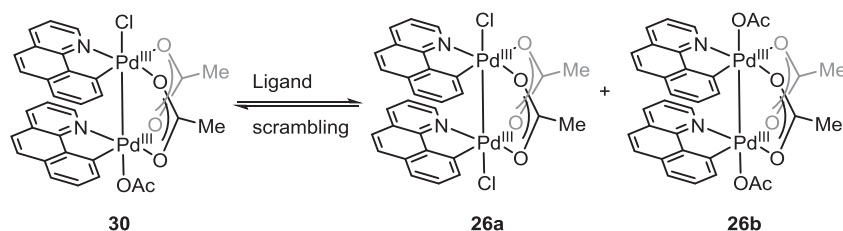


Fig. 15 Ligand scrambling demonstrated for a dinuclear Pd^{III} complex bearing benzo[*h*]quinoline ligands.

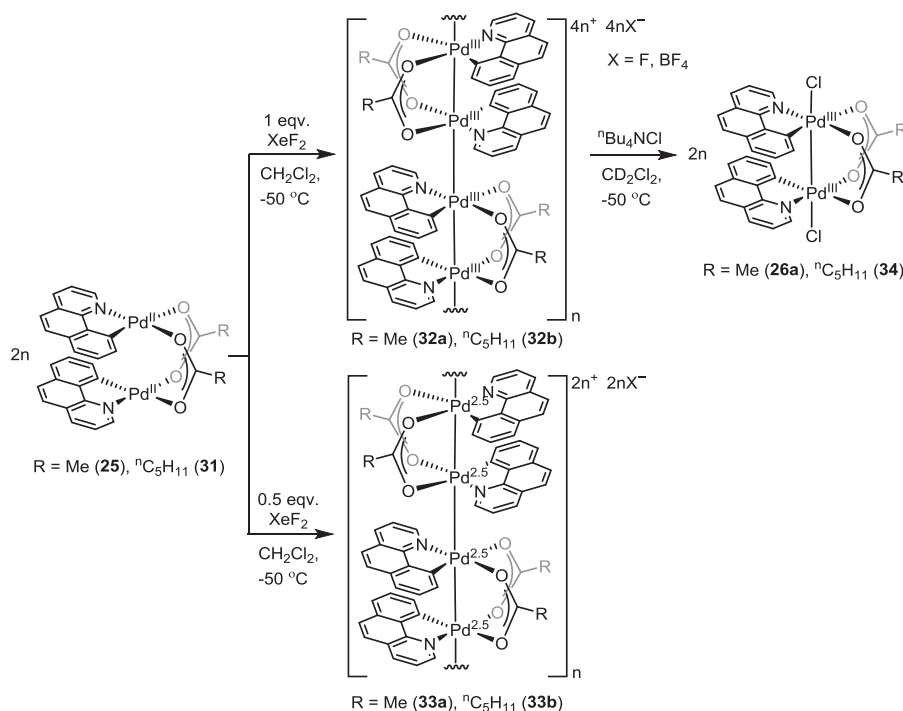


Fig. 16 Molecular 1D chains containing Pd^{III}–Pd^{III} bonds.

molecular wires **32a-b** in CD_2Cl_2 solution at -50°C yielded the dinuclear Pd^{III} species **26a** and **34** selectively. Interestingly, these Pd^{III} molecular chains bear semiconductor properties where bandgap can be tuned by changing the counterions and bridging carboxylates. Additionally, metallic conductivity based on an unusual average metallic oxidation state of 2.5 was observed for **33a-b** above 200 K.

6.10.2.2.4 Pd^{III} complexes featuring no $\text{Pd}^{\text{III}}-\text{Pd}^{\text{III}}$ bonds

6.10.2.2.4.1 Pd^{III} complexes stabilized by the tridentate Me_3tacn ligand

In 2011, the Mirica group reported a series of dinuclear Pd^{III} complexes, **36**, stabilized with the tridentate N,N',N'' -trimethyl-1,4,7-triazacyclononane (Me_3tacn) ligand (Fig. 17). These complexes represented the no direct $\text{Pd}-\text{Pd}$ bonds were observed, instead a single halide ion is bridging the two Pd^{III} centers, which are antiferromagnetically coupled.³⁶ Both Pd^{III} centers adopt a distorted octahedral geometry, with the bridging halide and the N donors *trans* to it defining the axial axis. These complexes are the first group 10 d^7-d^7 dinuclear complexes bridged by a single unsupported halide ligand and represent a model of the delocalized exhibit a linear $\text{Pd}^{\text{III}}-\text{X}-\text{Pd}^{\text{III}}$ electronic structure that has been proposed to exist in some $-\text{Pd}-\text{X}-\text{Pd}-\text{X}-$ one-dimensional (1D) chains. Interestingly, these dinuclear Pd^{III} complexes can be reversibly oxidized to mononuclear Pd^{IV} complexes, as discussed below in Section 3.2.1.

6.10.2.2.4.2 Pd^{III} complexes stabilized by bidentate ethylenediamine ligands

A 1D molecular chain containing $-\text{Pd}^{\text{III}}-\text{Br}-\text{Pd}^{\text{III}}-\text{Br}-$ units, **39**, was reported by Takaishi, Yamashita, and co-workers (Fig. 18).³⁷⁻³⁹ The unique features of this system are that the $-\text{Pd}-\text{X}-\text{Pd}-\text{X}-$ 1D molecular chains consist of N-donor ligands such as ethylenediamine and exhibit average $\text{Pd}-\text{Br}$ bond lengths of 2.608 Å and $\text{Pd}-\text{Pd}$ distances of 5.2 Å at temperatures below 200 K.

6.10.2.2.4.3 Pd^{III} complexes stabilized by pentaphenylferrocenyl imidazole or oxazoline ligands

In 2012, Peter and coworkers reported the chemical or electrochemical oxidation of chloride-bridged Pd^{II} complexes supported by pentaphenylferrocenyl imidazole or oxazoline ligands to generate the dinuclear Pd^{III} complexes **41** and **43**. Depending on the oxidant used, two chlorides, acetates, or nitrates can bridge between the two Pd^{III} centers, as shown by X-ray crystallography (Fig. 19).⁴⁰ The EPR spectra recorded for such Pd^{III} complexes at 110 K both in the solid and frozen state revealed an average *g* value of 2.340 with a large anisotropy. These results are attributed as Pd^{III} character, although the unpaired electron of the low-spin metal center resides in the d_{yz} orbital, rather than d_{z^2} orbital.

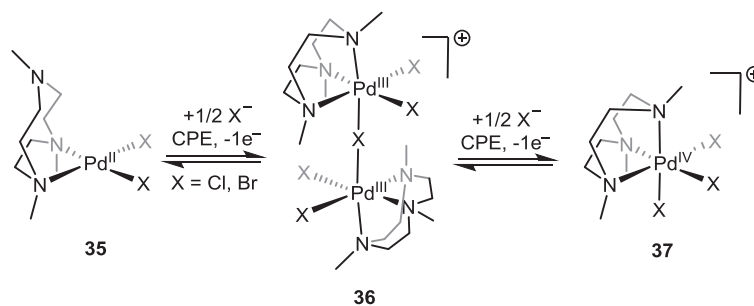


Fig. 17 Synthesis of dinuclear Pd^{III} and mononuclear Pd^{IV} complexes stabilized by the Me_3tacn ligand.

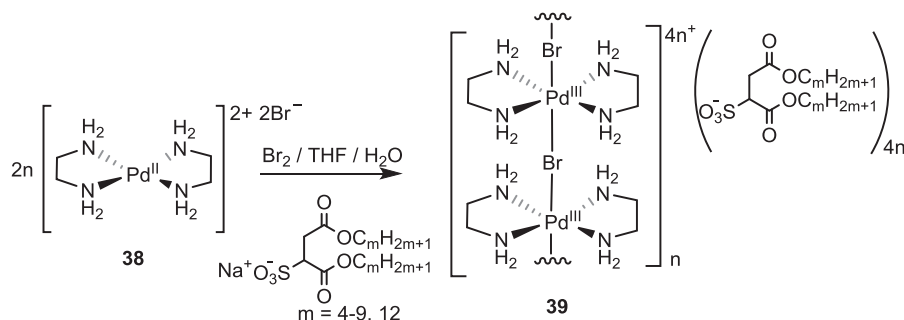


Fig. 18 Molecular 1D chains containing $\text{Pd}^{\text{III}}-\text{Br}-\text{Pd}^{\text{III}}$ bonds.

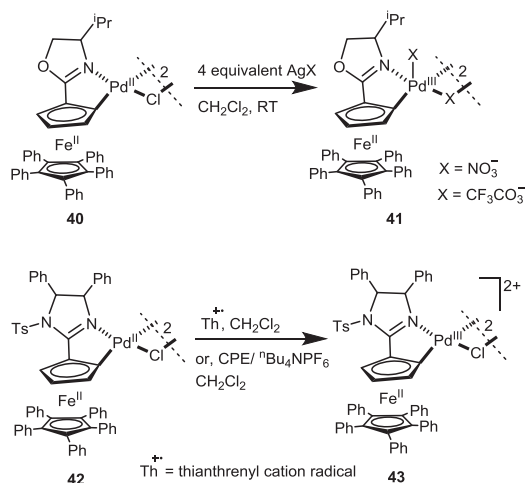


Fig. 19 Dinuclear Pd^{III} complexes supported by pentaphenylferrocenyl imidazole or oxazoline ligands.

6.10.3 Pd^{IV} Complexes

Pd^{IV} centers, as outlined in the introduction, prefer an octahedral coordination environment. Most ligand systems that have been used to stabilize these complexes feature fairly strong field ligands, and often contain a Pd–C bond. The chelate effect is often used to form stable complexes, and it is common to see bidentate or tridentate C/N-donor ligands being used to isolate these reactive species. Non-organometallic Pd^{IV} complexes with neutral donors such as NH₃, ethylenediamine (en), or halogeno complexes like [PdX₆]²⁻ (X = F, Cl, Br) had been studied in the 20th century. Interest in Pd^{IV} complexes has grown in the 1980s and 1990s, and observed or isolated Pd^{IV} species have been reported by the groups of Yamamoto, Canty, van Koten, and others.

We have classified the complexes according to the nature of the supporting ligand framework. The donor atoms are usually C, N, or O. The main classes of ligands that have shown the ability to support Pd^{IV} are as follows: (a) bidentate ligands such as bipyridine and terpyridine, which provide a strong chelation effect; (b) conformationally flexible ligands such as pyridinophanes, which can stabilize multiple oxidation states by changing their binding mode when interacting with the Pd center; (c) tridentate facially chelating ligands such as scorpionates that provide steric protection to the metal center as well as enhance its stability via the chelate effect; (d) tridentate planar ‘pincer’ ligands that have been widely employed to stabilize various metal centers; and (e) other various ligands that have been shown to stabilize Pd^{IV} centers.

Apart from well-defined molecular complexes which are of interest to the synthetic inorganic or organometallic community, Pd^{IV} has also been seen in halogen-bridged mixed-valence complexes such as [Pd(en)₂][PdBr₂(en)₂](C₇H₁₅SO₃)₄ and [Pd(en)₂Br](C_n-Y)₂·H₂O,^{37,41,42} which exhibit interesting physical properties such as intense and dichroic inter-valence charge-transfer bands, progression in the resonance Raman spectra, and luminescence spectra with large Stokes shifts. A related compound was synthesized by Edwards et al. in 2004,⁴³ which contained two Pd^{IV} centers ligated by bridging chloro- groups and two phosphide groups, along with two Pd⁰ centers. The crystal structure shows a C_{2v} geometry with the phenyl rings pointing outwards (Fig. 20).

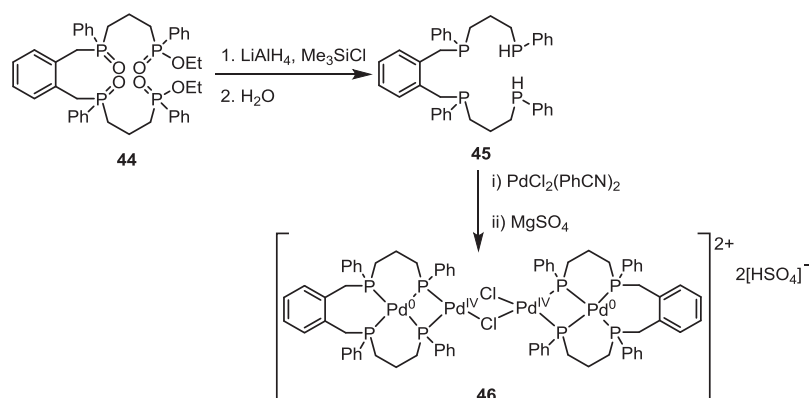


Fig. 20 Multinuclear Pd^{IV} complexes with phosphide ligands and bridging chlorides.

6.10.3.1 Pd^{IV} Complexes Stabilized by Bidentate Ligands

6.10.3.1.1 Pd^{IV} complexes stabilized by bipyridyl and 2-phenylpyridyl ligands

In 2002, Canty et al. reacted the neopentyl- and the trimethylsilylmethyl-Pd^{II} complexes **47a** and **47b** with 8-bromomethylquinoline to isolate Pd^{IV} complexes **48a** and **48b** (Fig. 21).⁴⁴ The C, N donor atoms of 8-bromomethylquinoline stabilized the Pd^{IV} center. The product was fully characterized by NMR, EA, and X-ray crystallography. The closely related silicon analog, where the starting compound had a trimethylsilyl group instead of t-butyl, was also characterized by NMR and EA. The Pd–C bond is *trans* to a bipyridine nitrogen, indicating the stronger *trans*-influence of the phenyl group, which would have otherwise destabilized the complex. The authors attributed the stability of these complexes to two factors: the influence of the chelators (bpy and 8-bromomethylquinoline), which precluded decomposition pathways via 5-coordinate species, and the steric bulk of the neopentyl or trimethylsilylmethyl and bidentate chelation of the aforementioned ligands prevent the formation of appropriately oriented transition states for C–C reductive elimination.

One of the earliest reports of the reaction between a Pd^{II}-alkyl species and hypervalent iodine reagents was from Canty and coworkers.⁴⁵ They reacted (bpy)Pd^{II}Me₂ with the hypervalent iodine reagent [IPh₂][OTf] to get a mixture of products with a complex NMR spectrum that indicated the presence of PdIME₃(bpy), PdMePh(bpy), and PdIME₂Ph(bpy), by comparison to literature reported spectra (Fig. 22). The presence of the trimethyl complex indicated methyl transfer reactions, which are often invoked in organopalladium(IV) chemistry.

In order to arrest the methyl transfer reactions, they reacted a palladacycle **50** with [IPh₂][OTf]. This generated the *cis* and *trans* isomers of a Pd^{IV} species **51** and **52** in a 1:1 ratio (Fig. 22). Yet again, it is interesting to note that none of the Pd–C bonds are *trans* to one another, showing the importance of bidentate chelation and negating unfavorable *trans*-influence in high-valent palladium chemistry. These reactions were all carried out at –50 °C, and the products were too unstable to be characterized by crystallography. However, salt metathesis with NaI allowed the isolation and structural characterization of *trans* iodide complex **53a**. Various alkane and olefin decomposition products were reported at ambient temperature, indicating facile reductive elimination processes.

The Sanford group pioneered the catalytic reactivity and mechanistic analysis of Pd^{IV} complexes supported by bidentate chelating ligands. The earliest report from the group detailed the synthesis and characterization of a series Pd^{IV} complexes with 2-phenyl pyridine ligands and aryl carboxylates from a 'C₂N₂O₂' type of donor atom set.⁴⁶ The *p*-NO₂ benzoate analog **56** was characterized by X-ray crystallography (Fig. 23). A variety of electronically diverse complexes (by varying the substituents on the benzoic

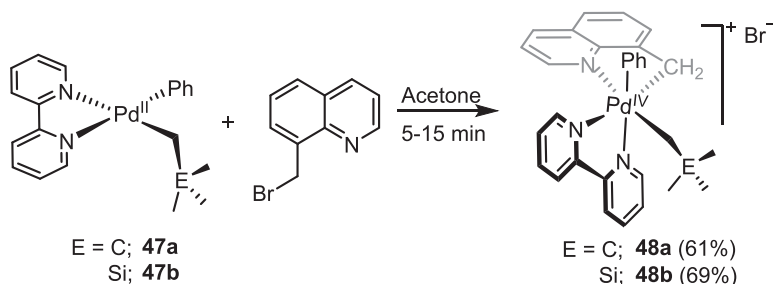


Fig. 21 Pd^{IV} complexes supported by the bipyridyl (bpy) ligand.

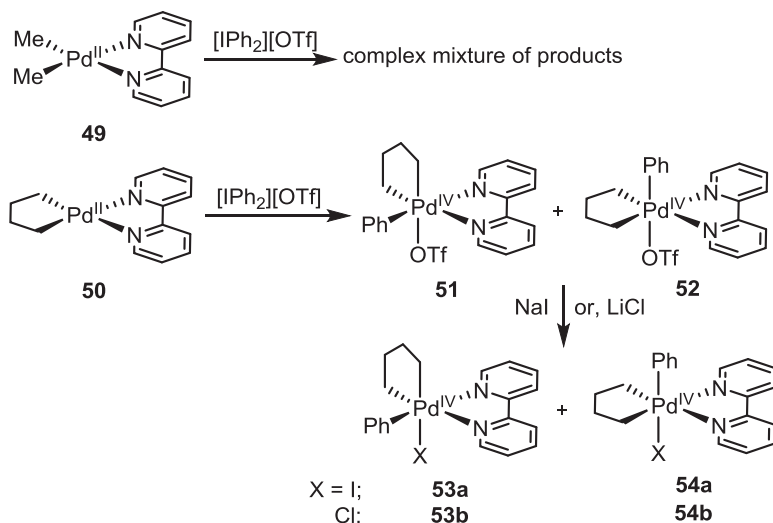


Fig. 22 Synthesis of bpy-supported Pd^{IV} complexes via oxidation by hypervalent iodine reagents.

acid or the phenyl pyridine) were synthesized. These complexes undergo reductive elimination to form C–O bonds, and mechanistic studies confirmed that the dissociation of either the carboxylate or the pyridine nitrogen is facile, due to the strong *trans*-effect of the phenyl group.

Aryl halides are key precursors for many industrially, agriculturally, and pharmaceutically relevant molecules. Hence, Sanford and co-workers further explored the 2-phenyl pyridine motif to explore the C–Cl bond formation reactivity of Pd^{IV} complexes. To investigate the possible role of Pd^{IV} intermediates in C–Cl bond formation, they characterized two complexes having a Pd^{IV}–Cl bond by reacting to the Pd^{II} complex with PhICl₂ and N-chlorosuccinimide (NCS, Fig. 24).⁴⁷ The Pd^{IV} complex formed by the reaction of 55 with NCS was also characterized by X-ray crystallography and was the first example of an oxidative addition into the N–Cl bond of an N-halosuccinimide. The NMR spectrum of complex 57 showed characteristic features of a Pd^{IV} complex bearing *cis* Cl coordination and two inequivalent phenyl pyridine groups. It showed remarkable thermal stability in solid-state, for at least 2 weeks. The solid-state structure of 58 shows that the weak field chloride is *trans* to a pyridine ligand while the succinimide is *trans* to a σ -phenyl group, in line with the stronger *trans* influence of the σ -phenyl group. Thermolysis of these Pd^{IV} complexes afforded important insights into C–C and C–Cl bond formation reactivity.

The Malinakova group made use of the bipyridine ligand to isolate a Pd^{IV} complex *en route* to a cyclization reaction.⁴⁸ The palladacycle with a stereogenic carbon was reacted with a substituted allyl bromide to form the Pd^{IV} complex 60 (Fig. 25). The crystal structure revealed a distorted octahedral complex with the Pd forming a five-membered chelate ring with the phenyl-*o*-(ethoxycarbonylmethyleneoxo) group.

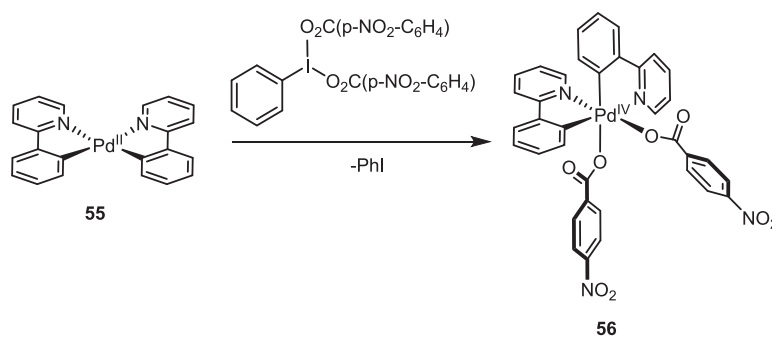


Fig. 23 Pd^{IV}-Carboxylate complexes supported by phenylpyridyl ligands.

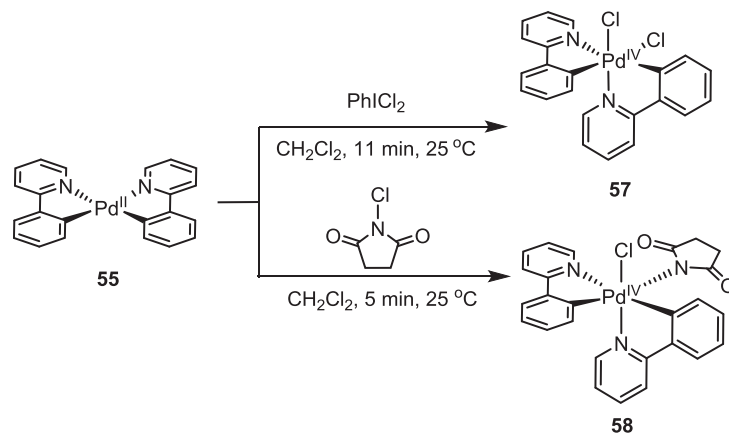


Fig. 24 Pd^{IV}-Cl complexes supported by 2-phenylpyridyl ligands.

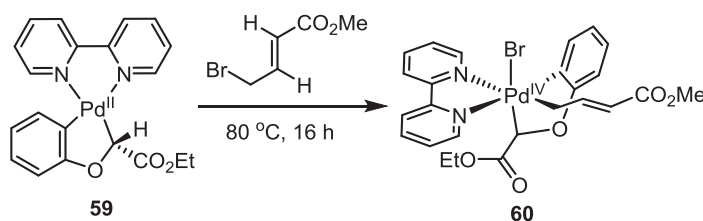


Fig. 25 Synthesis of a Pd^{IV} η^1 -allyl complex.

The first example of an organometallic Pd^{IV} difluoride complex came from the exploration of aromatic C–H fluorination by the Ritter group (Fig. 26).⁴⁹ Hypothesizing the presence of a high-valent palladium intermediate during the reductive elimination to furnish a C–F bond, they made use of a rigid chelating benzoquinolinyl ligand to stabilize a putative Pd^{IV}-fluoride intermediate. Treatment of the Pd^{II} precursor with Selectfluor generated an intermediate 62, which was characterized by ¹H, ¹⁹F, and ¹³C NMR spectroscopy. A resonance at –278 ppm in the ¹⁹F spectrum was consistent with the assignment of a Pd^{IV}–F species. Treatment of the intermediate with tetramethylammonium fluoride tetrahydrate generated the complex 63, which was also independently synthesized by a reaction with XeF₂ and structurally characterized. The Pd–F bond lengths of 1.955(3) Å and 2.040(3) Å were consistent with a Pd^{IV} assignment.

Further studies of the aryl fluorination chemistry were carried out by the Sanford group. They were able to isolate and characterize the Pd^{IV} complex 65 as the product of the fluorination reaction of the bipyridyl-Pd^{II} complex 64 with XeF₂ (Fig. 27).⁵⁰ Notably, unlike the previous example, complex 65 did not require the presence of two chelating ligands to stabilize the high valent Pd^{IV} center. The axial Pd–F bond (2.113 Å) is considerably longer than the equatorial ones (~1.930 Å), indicating a combined *trans* influence of the σ-aryl bond and the hydrogen bonding by the HF, which the authors ascribed to being generated by the reaction of XeF₂ with adventitious water.

To examine the C–F reductive elimination reactivity of cyclometalated Pd^{IV} complexes, Sanford and co-workers synthesized several Pd^{IV}-cyclonophyl complexes 67–70 supported by the bipyridyl ligand (Fig. 28).^{31,51} The triflate group, *trans* to the σ-alkyl group, is labile and could be substituted with a variety of *trans*-axial ligands. Complex 68 with the aquo ligand was characterized by X-ray crystallography. It was found that these complexes showed the formation of a C_{sp³}–F bond, in contrast to the usual C_{sp²}–F bond formation observed in Pd^{II} chemistry, yet again highlighting their complementary reactivity.

In order to investigate the mechanism of the competition between C_{sp³}–N and a C_{sp³}–F bond formation, the Sanford group synthesized a model Pd^{IV} complex 67 (Fig. 29).⁵² They found that thermolysis of the major isomer led to a mixture of sp³ C–N, sp³ C–F and C_{sp²}–C_{sp³} reductive elimination products, while adding excess [NMe₄][NHTs] and bipyridine led to an increased selectivity for the C–N bond formation reaction.

The Dong group isolated the first complexes containing a Pd^{IV}-sulfinate group in 2011 (Fig. 30).⁵³ They sought to explore the direct C–S reductive elimination to form sulfones from a high-valent palladium intermediate. Oxidative addition of various sulfonyl chlorides to 2-phenyl pyridine-Pd^{II} complexes generated Pd^{IV} complexes, of which the ones bearing *p*-Me (73) and *p*-OMe (74) groups were isolated and characterized by X-ray crystallography. Thermolysis of these Pd^{IV} species generated a mixture of C–C and C–S reductive elimination products. Analogous benzoquinoline-ligated palladium(IV) sulfinate complexes showed higher selectivity toward the formation of a C–SO₂ bond.

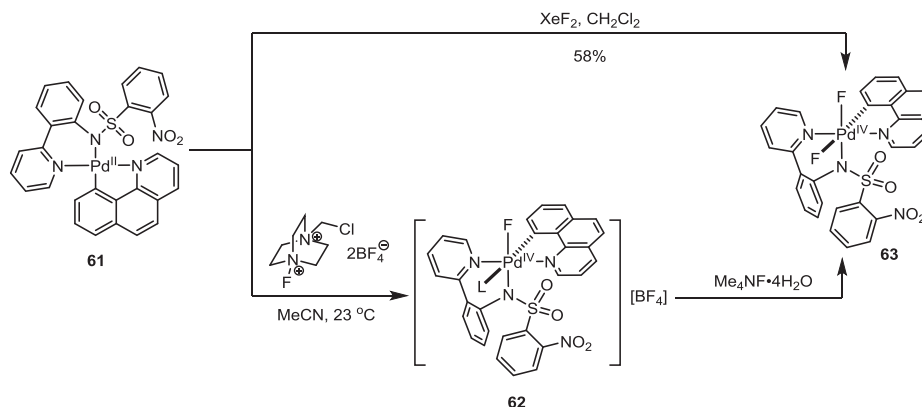


Fig. 26 An organometallic Pd^{IV}–F complex supported by a benzoquinolinyl ligand.

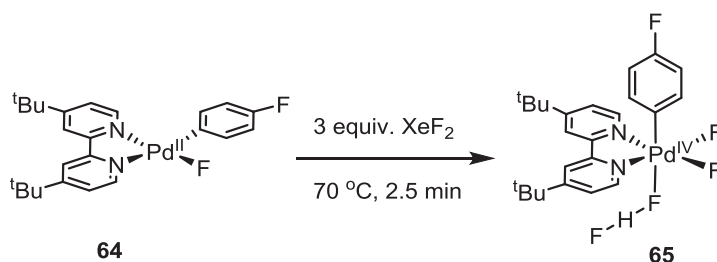


Fig. 27 A (^tBubpy)Pd^{IV} complex with a Pd^{IV}–F bond.

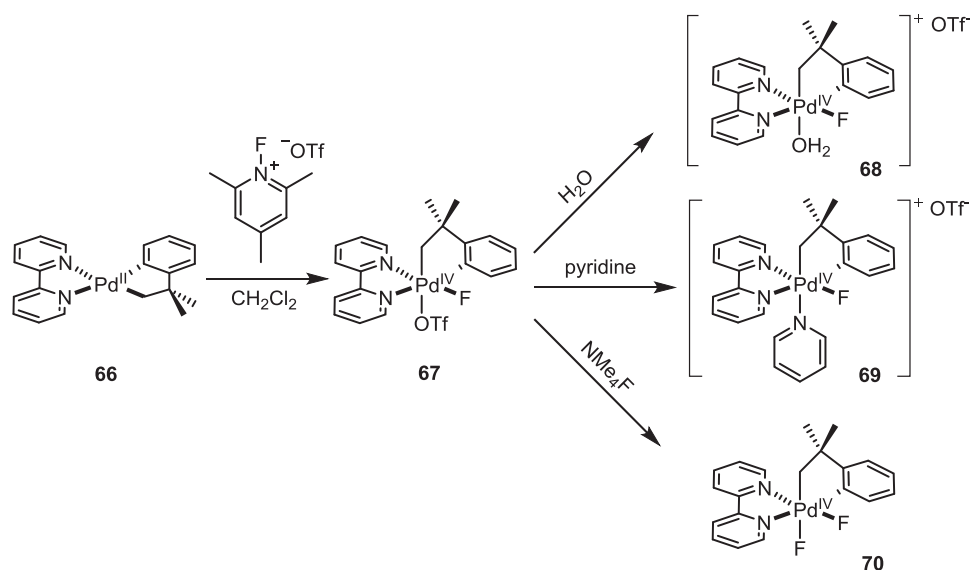


Fig. 28 Pd^{IV}-Cycloneophyl complexes used in C–F bond formation reactions.

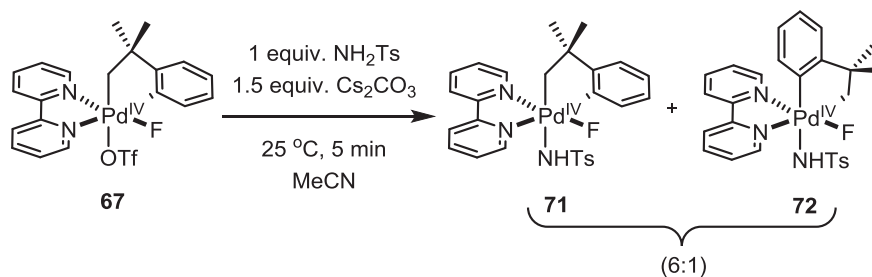


Fig. 29 Additional Pd^{IV}-F complexes used in C–F bond formation reactions.

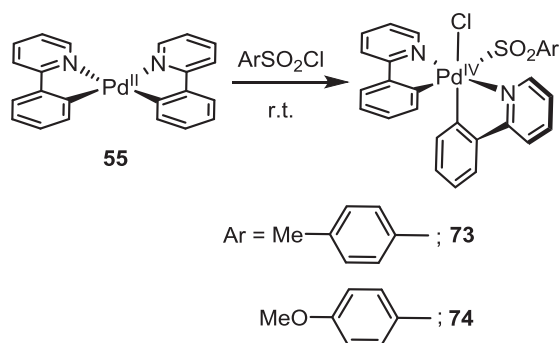


Fig. 30 Pd^{IV}-sulfinate complexes supported by 2-phenylpyridyl ligands.

The scope of the reactivity of the (bipyridyl)Pd^{IV} systems was extended to aryl trifluoromethylation by the Sanford group in 2010 (Fig. 31).³⁰ Interestingly, they found the use of oxidants like PhI(OAc)₂, NBS, or NCS did not promote C_{aryl}-CF₃ bond formation. The preferred pathway was reductive elimination to form halogenation or acetoxylation products. The authors reasoned that using *N*-fluoro-2,4,6-trimethylpyridinium triflate would be a better alternative as it would introduce fluoride and triflate ligands to the Pd^{IV} center that would be less prone to reductive elimination. This was in fact the case, and they were able to obtain X-ray quality crystals of the Pd^{IV} complex 76 with a trifluoromethyl group. Extensive mechanistic studies led them to propose that the C_{aryl}-CF₃ bond formation takes place from a pentacoordinate intermediate, and CF₃ serves as the electrophilic partner during the bond formation.⁵⁴

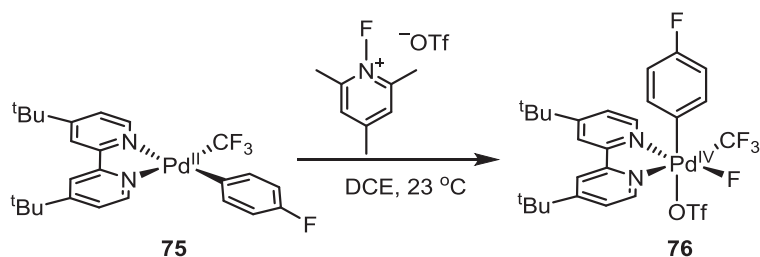


Fig. 31 Synthesis of a Pd^{IV}-CF₃ complex.

Though C–H activation at Pd^{IV} centers has been invoked previously, there were no examples of isolated Pd^{IV} complexes that can undergo C–H bond activation. The Sanford group reasoned that slowing down the competing reductive elimination could facilitate the isolation of a C–H activated Pd^{IV} complex. To this end, they employed the trifluoromethyl group and a bipyridyl ligand, both known to hinder reductive elimination. Upon oxidizing the Pd^{II} complex 77 with various oxidants, they were able to isolate the octahedral complex 79-TFA with a TFA ligand and characterize it crystallographically (Fig. 32).⁵⁵ The other Pd^{IV} complexes 79 were also characterized by NMR.

In the same vein as the pincer complexes reported from the Bautista group, which are discussed later in the chapter, the pre-positioning of an aryl halide in close proximity to a Pd^{II} center facilitates its oxidative addition to form a stable, isolable Pd^{IV} complex 81. Treating the Pd^{II} precursor with thallium acetylacetonate led to dehydroiodination and the formation of an unusual NCC pincer complex. The greater *trans* influence of a C- vs a N-donor ligand is observed in an asymmetry of the Pd–N_tBu₂ppy bond distances (2.176 vs. 2.077 Å) (Fig. 33).

6.10.3.1.2 Pd^{IV} complexes stabilized by terpyridyl ligands

The Amatore group saw evidence for the formation of phenanthroline-supported norbornane-Pd^{IV} complexes 83 in the cyclic voltammogram of the Pd^{II} complex 82 in the presence of a benzyl halide (Fig. 27).⁵⁶ The CV of complex 82 exhibited an oxidation peak at +0.795 V versus SCE, which disappeared on the addition of excess benzyl halide, suggesting the formation of an oxidative addition product. Complexes of this type, the authors noted, have been characterized previously by NMR spectroscopy by Catellani and coworkers (Fig. 34).

The usual strategy for stabilizing Pd^{IV} complexes has been the use of strong chelating ligands and strong σ-donors to stabilize the high-energy metal d-orbital manifold. The σ-donors have mostly been alkyl groups. The Sanford and Arnold groups, in 2009, employed a N-heterocyclic carbene (NHC) ligand to stabilize a Pd^{IV} complex 85 formed by the oxidative addition of the Pd^{II} complex 84 with PhICl₂ (Fig. 35).⁵⁷ The complex was fully characterized by NMR spectroscopy and X-ray diffraction. NHCs are highly tunable and offer significant versatility in sterics and electronics to facilitate stereo- and enantioselective organic

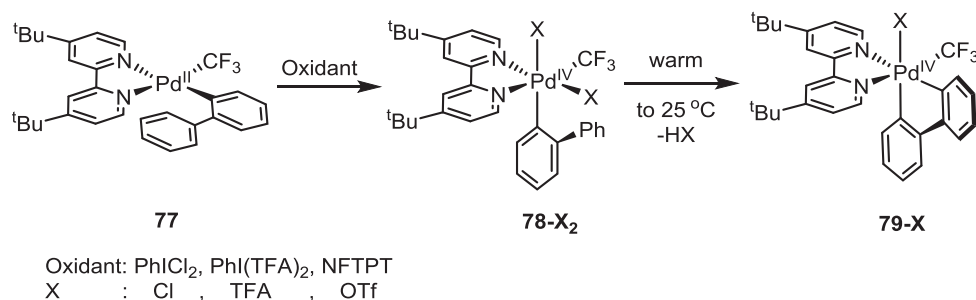


Fig. 32 A Pd^{IV} complex formed upon C–H bond activation.

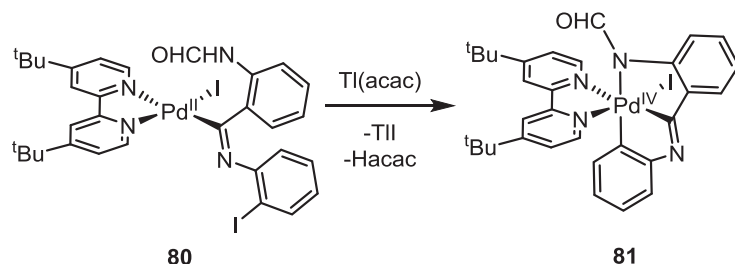


Fig. 33 Synthesis of an NCC pincer Pd^{IV} complex via oxidative addition of an aryl iodide.

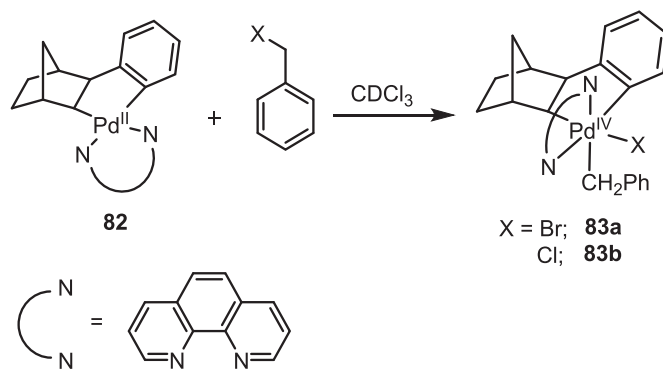


Fig. 34 Formation of norbornane-Pd^{IV} complexes supported by phenanthroline.

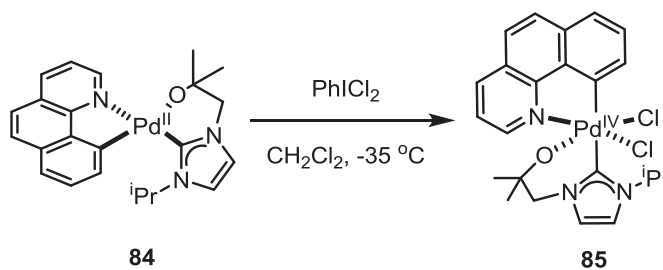


Fig. 35 Formation of an NHC-supported Pd^{IV}-dichloro complex.

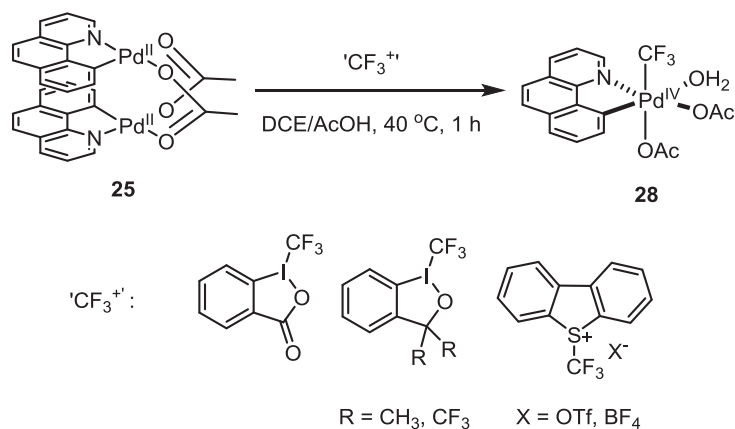


Fig. 36 Formation of a Pd^{IV}-CF₃ complex via electrophilic trifluoromethylation of a Pd^{II} precursor.

transformations. The dichloro complex **85** was shown to be competent in C–Cl bond-forming reactions, and the Pd–C(NHC) bond was shown to be stable in strongly oxidizing conditions.

The oxidation of Pd^{II} dinuclear complexes to form dinuclear Pd^{III} complexes has been implicated in C–H arylation reactions as the rate-determining step. Such dinuclear Pd^{III} complexes have, in fact, been isolated (see [Section 2.2](#) in this chapter). In addition, mononuclear Pd^{IV} complexes are also viable intermediates in the proposed catalytic cycles, and Sanford and co-workers were able to isolate a Pd^{IV} complex **28** by the reaction of **25** with the electrophilic trifluoromethylation reagents listed ([Fig. 36](#)). The solvent was found to play a crucial role, with reactions in acetic acid producing high yields of the complex **28**. The weak field aqua ligand is *trans* to the σ -aryl group, yet again demonstrating the impact of the *trans* influence in stabilizing these complexes. This finding indicates that a definitive identification of the high-valent Pd intermediates involved such oxidative reactions is dependent on a multitude of factors.

In 2012, the Sanford, Canty, and Ritter groups reported a detailed kinetic analysis of the possible high-valent palladium intermediates.³¹ It has been experimentally observed that oxidation of **25** with PhICl₂ or PhI(OAc)₂ leads to isolable dinuclear Pd^{III} complexes ([Fig. 12](#)). On the other hand, the oxidation of **25** with Togni's reagent leads to the formation of the Pd^{IV} complex **28**

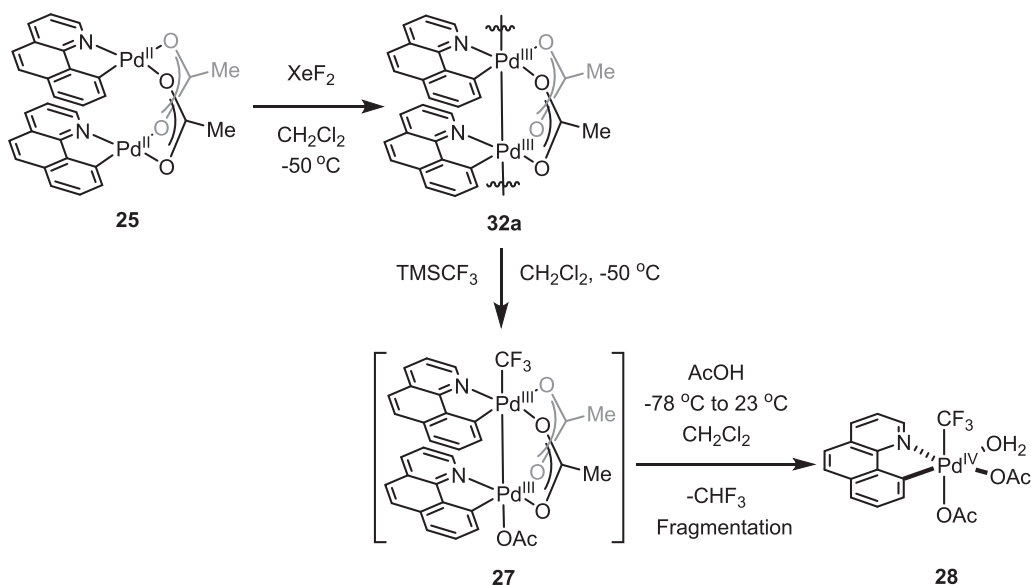


Fig. 37 Pd^{III} and Pd^{IV} complexes supported by the benzoquinoyl ligand.

(Fig. 36). These seemingly disparate results were united by theoretical calculations and experimental evidence. Treatment of the 1D molecular wire 32a with TMSCF₃ resulted in the formation of a transient dinuclear Pd^{III} complex 27, which was characterized by comparing its NMR spectrum to the analogous oxidation products with other TMSX (X = Cl, OAc) reagents. A resonance at 2.74 ppm, which is diagnostic of the acetate bridge, helped establish its identity unequivocally. Upon warming up 27 in the presence of 10 equivalents of AcOH, the Pd^{IV} complex 28 was formed. This established the viability of a Pd–Pd heterolysis step and showed that the dinuclear Pd^{III} and mononuclear Pd^{IV} complexes are intimately connected (Fig. 37).

6.10.3.2 Pd^{IV} Complexes Stabilized by Conformationally Flexible Ligands

6.10.3.2.1 Pd^{IV} complexes stabilized by the Me₃tacn ligand

In 2011, Mirica and co-workers isolated Pd^{III} and Pd^{IV} complexes supported by similar ligand environments (Fig. 17),³⁶ further adding credence to the hypothesis that there may be multiple possible high-valent Pd intermediates involved in various reactions. The conformationally flexible Me₃tacn ligand was used to stabilize both Pd^{III} and Pd^{IV} complexes: while the dinuclear Pd^{III} complexes 36 exhibit a bridging halide ligand and the Pd^{III} centers adopt a Jahn-Teller-like distorted geometry, the mononuclear Pd^{IV} complexes 37 adopt a pseudo-octahedral geometry, with two facial triads being formed by the tacn ligands and three halides, respectively. It was shown that the Pd^{IV} species exhibited slow decay or underwent comproportionation with the Pd^{II} complex to form the Pd^{III} species. Thus, the three complexes are interconvertible by controlled potential electrolysis, with the Pd^{III} dinuclear complex showing exceptional stability. The complexes were all characterized by X-ray crystallography, while their interconversions were studied using UV-vis spectroscopy and electrochemistry.

The Me₃tacn ligand scaffold was further used to probe the aerobic oxidation reactivity of high-valent Pd complexes.⁵⁸ The reaction of the (Me₃tacn)Pd^{II}Me₂ complex (86) with dioxygen resulted in the formation of (Me₃tacn)Pd^{IV}Me₃ (87), one of the first isolated and crystallographically characterized Pd^{IV} complex formed as a result of aerobic oxidation (Fig. 38). ESI-MS confirmed the presence of high-valent palladium adducts with reduced dioxygen species (superoxide, hydroperoxide, hydroxide), which are often invoked as elusive reaction intermediates. The fact that these high-valent intermediates had a longer lifetime in protic solvents

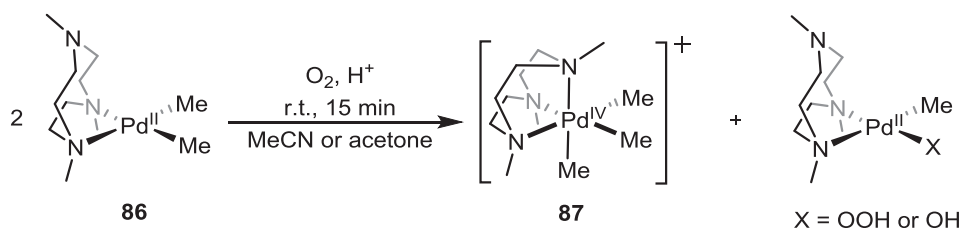


Fig. 38 Generation of a Pd^{IV}-trimethyl complex upon aerobic oxidation of a Pd^{II}Me₂ precursor supported by the Me₃tacn ligand.

indicated the inner-sphere nature of the reaction. The Pd^{IV}-trimethyl complex **87** was likely produced via a methyl group transfer from an electrophilic Pd^{IV}Me₂X (X = OOH, OH) to a Pd^{II} complex, a mode of reactivity well established in the aerobic reactivity of Pd- and Pt-methyl complexes.

To circumvent the problem of methyl group transfer, Mirica and co-workers carried out the aerobic oxidation of a Pd^{II} cycloneophyl complex **88** supported by the Me₃tacn ligand (Fig. 39).⁵⁹ Because of the additional stability afforded by the five-membered palladacycle, the Pd^{IV}-OH complex **89** could be isolated and characterized by NMR, X-ray crystallography, and ESI-MS. In accordance with previously established reactivity and the rapid oxidation reaction in the presence of protons, an inner sphere oxidation of the Pd^{II} complex by O₂ was invoked. Furthermore, the thermolysis of complex **89** led to the formation of 2-*tert*-butylphenol via reductive elimination.

6.10.3.2.2 Pd^{IV} complexes stabilized by pyridinophane ligands

As discussed above, the Mirica group has employed conformationally flexible tetradentate pyridinophane ligands RN4 to stabilize Pd centers in different oxidation states.¹³ The electronic structure and organometallic reactivity of these complexes were thoroughly characterized. The basic idea behind these ligands is that they have pendant donors that can bind axially to form octahedral or distorted octahedral complexes in response to a change in the electronic structure of the complexes.

The oxidation of (RN4)Pd^{II} complexes to (RN4)Pd^{III} species was carried out by both chemical and electrochemical means (Fig. 2), and selected Pd^{III} species could be further oxidized to the Pd^{IV} complexes **90–93** (Fig. 40). Interestingly, it was observed that the oxidation potentials increase with the steric bulk of the R group, which was rationalized by the inability of the bulkier N-substituents to stabilize the more symmetric octahedral geometries of the Pd^{IV} centers. From the crystal structures of these complexes, it was found that the Pd–N_{axial} bonds were longer for the Pd^{III} complexes **1–3** than for the Pd^{IV} complexes **90–93** by 0.24–0.27 Å, in line with the Jahn-Teller distorted Pd^{III} centers. Indeed, this was confirmed by the EPR spectra of the Pd^{III} complexes, which show a d_z² ground state for the Pd^{III} centers.

While pyridinophanes had been previously used by the Mirica group to stabilize high-valent Pd, their efficacy in mediating aerobic oxidations at room temperature was reported in a later communication.¹³ Because of the conformational flexibility, the MeN4 ligands can change their denticity according to the electronic structure of the metal center, leading to low oxidation potentials and facile inner sphere oxidation by dioxygen in the presence of protic solvents, which can stabilize various high-valent Pd species containing reduced dioxygen ligands. For example, the [(MeN4)Pd^{III}Me₂]⁺ complex **3-Me** was characterized using UV-vis, ESI-MS, and EPR, which reveals a Jahn-Teller distorted octahedral geometry. Interestingly, the trimethyl Pd^{IV} complex [(MeN4)Pd^{IV}Me₃]⁺, **94**, was also detected by NMR during the aerobic oxidation of **91**, as well as independently synthesized and structurally characterized (Fig. 41), suggesting the presence a methyl group transfer step during the oxidation. The axial methyl group is substantially tilted towards the equatorial plane, away from the N–Me arm of the pyridinophane ligand, likely due to a steric clash of the methyl protons. In addition, various experimental techniques (EPR and ESI-MS) were used to verify the presence of reduced dioxygen adducts of high-valent Pd, providing key insights into the mechanism of aerobic oxidation of these complexes.

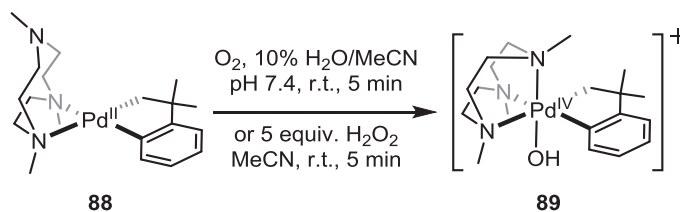


Fig. 39 A Pd^{IV} cycloneophyl complex stabilized by the Me₃tacn ligand.

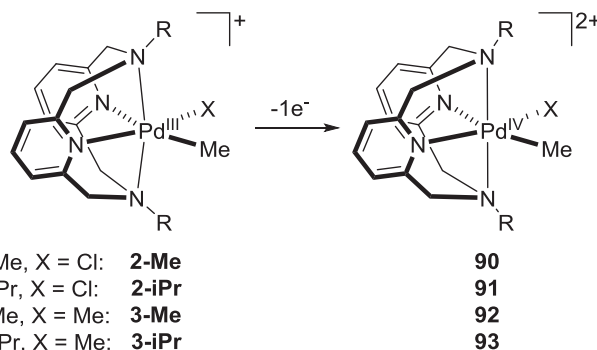


Fig. 40 Oxidation of (RN4)Pd^{III} complexes to generate (RN4)Pd^{IV} complexes.

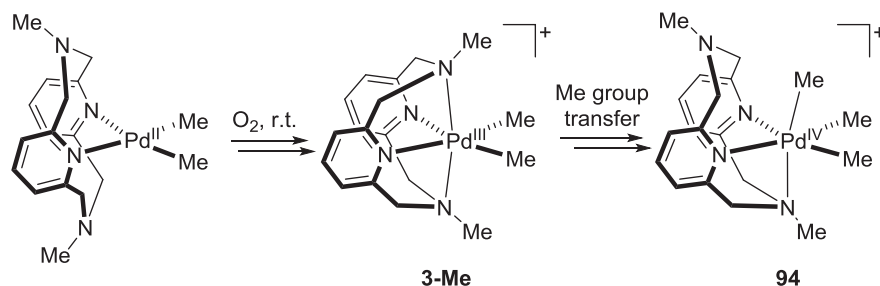


Fig. 41 Pd^{III}-dimethyl and Pd^{IV}-trimethyl complexes supported by MeN4.

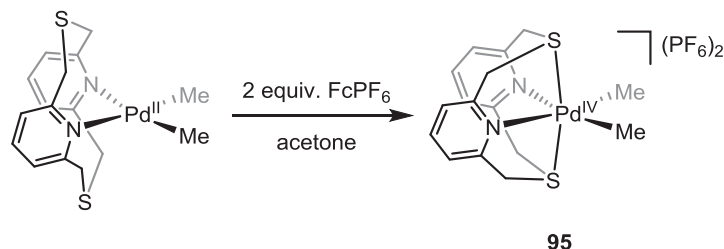


Fig. 42 A Pd^{IV}-dimethyl complex stabilized by the N2S2 ligand.

The Mirica group used the same pyridinophane ligand motif to synthesize a ligand scaffold with axial thioether donors.⁶⁰ Surprisingly, the soft thioethers were able to stabilize the Pd^{IV} complex **95**, which is the second example of an isolated, crystallographically characterized Pd^{IV} complex bearing thioether donors (Fig. 42). This highlights the role of steric effects in these ligands to stabilize Pd^{IV}. The more spherically symmetric N2S2, like the MeN4, is better suited to accommodate an octahedral geometry in comparison to the more sterically encumbered ^tBuN4 ligand.

6.10.3.3 Pd^{IV} Complexes Stabilized by Tridentate Facial Chelating Ligands

6.10.3.3.1 Pd^{IV} complexes stabilized by tris-(pyrazolylborate) (Tp) ligands

Tiripicchio and co-workers reported the formation of Pd nitrosyl complexes supported by a hydro(trispyrazolylborate) ligand, Tp.⁶¹ They also explored the reactivity of these complexes with dioxygen. A (Tp)Pd^{II}(cycloneophenyl) complex, **96**, was reacted with *N*-methyl-*N*-nitroso-*p*-toluenesulfonamide (Diazald) to produce the Pd^{IV} complex **97**, which was characterized by NMR and X-ray crystallography. According to the Enemark-Feltham notation, the complex can be written as {Pd(NO)}⁸, thus the nitrosyl ligand is expected to be bent. From the crystal structure, it was found that the Pd-N-O angle was 118.3(5)°, a distinctively bent nitrosyl ligand. This reaffirms the assignment of the formal oxidation state of Pd^{IV}. The reaction of **97** with oxygen yielded the Pd-nitrate compound **98** (Fig. 43), where the presence of a NO₃⁻ ligand was confirmed by IR. Treating a toluene solution of **98** with PMe₃ resulted in the formation of the cationic Pd^{IV} complex **100**, which was confirmed by an intense IR band at 1375 cm⁻¹ due to free nitrate. To check if the reaction proceeds through a nitro intermediate, **96** was oxidized with NO₂ to give another Pd^{IV} complex **99**, which when reacted with O₂ failed to produce **98**, suggesting that it may not be involved in the formation of the nitrate complex.

The reactivity of the (Tp)Pd^{II}(cycloneophenyl) complex **96** with dihalomethanes was studied by Valerga and co-workers (Fig. 44).⁶² Reaction was very slow with dichloromethane (complete conversion was achieved only after 36 h), yet it was extremely rapid with dibromomethane and diiodomethane, even at -78 °C. The product of the reaction with dichloromethane yielded the chloromethyl Pd^{IV} complex **103**, which was stable to decomposition even at 90 °C. The structure was established by COSY, HSQC, and HMBC NMR spectra. With CH₂I₂ and CH₂Br₂, a mixture of products was formed, with complex **101** being the major product and that was characterized by X-ray crystallography. The authors invoked a radical addition mechanism to explain the formation of the minor isomer **102**. Transient halomethyl Pd species were detected in the reaction mixture by NMR. This led the authors to suggest that a reductive coupling of the CH₂X fragment and the aryl group, followed by an intramolecular oxidative addition to the Pd^{II} center, could lead to the formation of the major isomer **101**.

The Alvarez group oxidized a (Tp)Pd^{II}(neophenyl) complex with two equivalents of [FcCp₂][PF₆] in the presence of an auxiliary pyridine ligand to form the Pd^{IV} complexes **104** (Fig. 45).⁶³ The role of the auxiliary ligand is to satisfy the octahedral coordination of the Pd^{IV} complex. The complexes were characterized by NMR and IR. Because the coordination environment around Pd^{IV} is inequivalent, the ¹H and ¹³C{¹H} NMR spectra exhibited three sets of signals for the inequivalent pyrazolyl rings, and diastereotopic CH₂ protons and methyl CMe₂ groups. Electrochemical experiments indicated a strong dependence of the irreversible Pd^{IV}-to-Pd^{III}

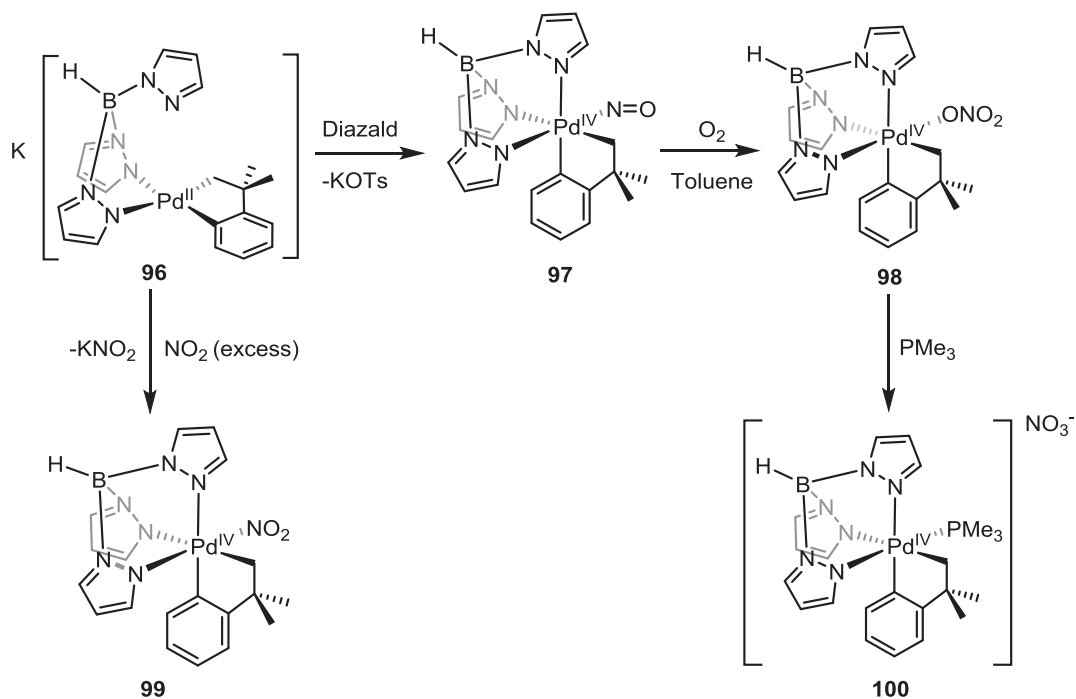


Fig. 43 Pd^{IV}-nitrosyl complexes supported by a Tp and a cycloneophyl ligand.

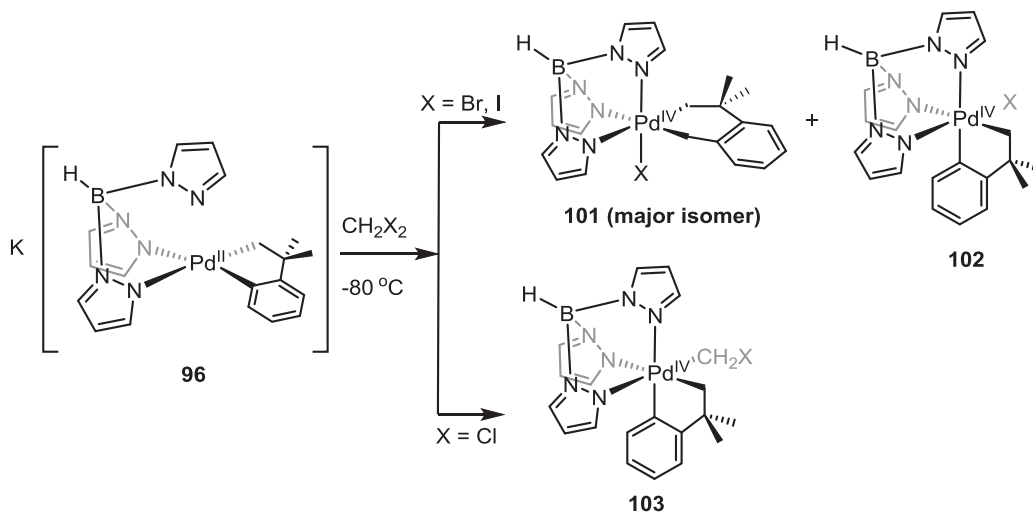


Fig. 44 Pd^{IV} complexes generated via the reaction of a (Tp)Pd^{II}(cycloneophyl) complex with dihalomethanes.

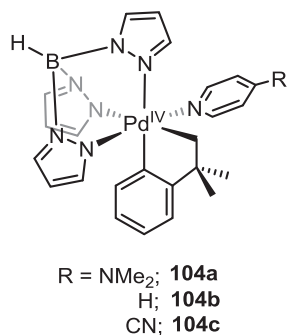


Fig. 45 (Tp)Pd^{IV}(cycloneophyl) complexes with equatorial pyridine derivatives.

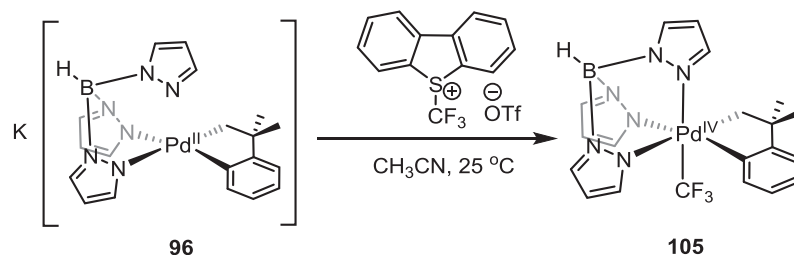


Fig. 46 A (Tp) Pd^{IV} (cycloneophyl) complex featuring a $\text{Pd}^{\text{IV}}\text{-CF}_3$ bond.

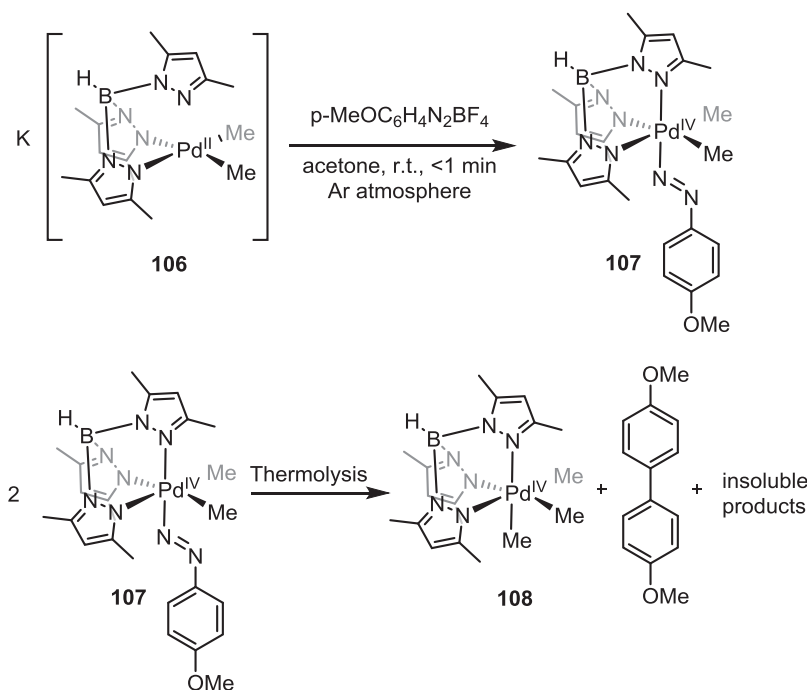


Fig. 47 Synthesis and reactivity of a (Tp*) Pd^{IV} aryl diazenido complex.

reduction wave on the nature of the R substituent on the pyridine, with the Pd^{IV} complexes with more electron withdrawing pyridine ligands leading to a more facile reduction.

The Sanford group also isolated a structurally related trifluoromethylated (Tp) Pd^{IV} (cycloneophyl) complex **96** (Fig. 46), in a study which compared the reactivity of this Pd^{IV} complex and its 3d congener Ni^{IV} complex.⁶⁴

Fekl and co-workers isolated an aryl diazenido Pd^{IV} complex **108** supported by the Tp* ligand and formed upon the oxidation of the Pd^{II} precursor **106** with an aryl diazonium salt.⁶⁵ The crystal structure of **108** revealed a doubly bent geometry for the aryl diazenido ligand, while the geometry around the Pd center was a slightly distorted octahedron (Fig. 47). The thermolysis of complex **108** revealed the formation of the trimethyl Pd^{IV} complex **109** (34%), arising from methyl group transfer between Pd^{II} and Pd^{IV} , along with 4,4'-dimethoxybiphenyl (36%) and an insoluble mixture of products, which would be expected to arise from the decomposition of in situ generated Pd^{II} complexes.

To explore the mechanistic nuances of the C–H bond activation at a Pd^{IV} center, the Sanford group substituted the bidentate bipyridyl ligand with a tridentate tris(2-pyridyl)methane ligand.⁶⁶ This increased the stability of the C–H activated complex which allowed them to investigate the steps of C–H activation in detail. In fact, the Pd^{IV} complex **111** was stable at room temperature in the solid-state for at least 4 weeks (Fig. 48). The authors noted that the phenyl ring of the biaryl ligand was positioned below the two pyridine rings of the ligand, stabilized by π -stacking interactions. In addition, the counteranions to the monocationic Pd^{IV} complexes were in intimate contact with the methine and pyridine protons. In addition, as a part of the mechanistic investigations, several Pd^{IV} complexes **110** were characterized either by X-ray crystallography or by NMR.

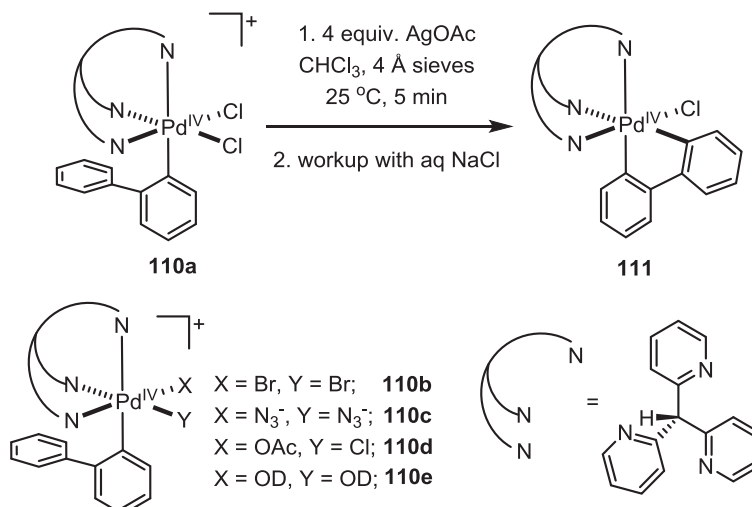


Fig. 48 Pd^{IV} complexes supported by a tris(2-pyridyl)-methane ligand.

6.10.3.3.2 Pd^{IV} complexes stabilized NNO or NCO donors based on diaryl ketones

The Vedernikov group employed a novel ligand to stabilize Pd^{IV} centers, comprising facial triads of N, N, O donors,⁶⁷ derived from di-2-pyridyl ketone and 2-aryl pyridine. The Pd^{IV} complexes **113** were formed upon treating the Pd^{II} complexes **112** with H₂O₂ (Fig. 49), and subsequent treatment with hydroxide yielded complexes **114**. The Pd^{IV} complexes **113a** and **114b** were fully characterized by NMR and X-ray crystallography. The complexes underwent reductive elimination when treated with excess base (KOH) or acids (HCl or HBr) and led to the formation of C–X bonds (X = Br, Cl, OH). The second set of complexes, without one of the facially chelating ligand triads, was more reactive (Fig. 50). This was presumably due to the ease of formation of a five-coordinate Pd^{IV} complex, where the Pd–N bond *trans* to the Pd–C is cleaved due to the stronger *trans*-influence of the σ -aryl bond.

The Vedernikov group also isolated the first examples of amido-aryl Pd^{IV} complexes **119**, which had been proposed by Gaunt as intermediates in C_{sp}²–N bond formation reactions.⁶⁸ Oxidation of the Pd^{II} complexes **118** bearing various substituents on the amido group eventually led to the formation of carbazoles as the C–N reductive elimination product. A hydroperoxoketal intermediate, formed by the initial oxidation of the di-(2-pyridyl)ketone was detected, which was subsequently oxidized to form Pd^{IV} complexes **119** (Fig. 51). These Pd^{IV} species were extremely short-lived when R was relatively electron-rich (Me, H, SO₂Me). However, the complex **119b** bearing a SO₂CF₃ substituent on the N-methanesulfonylamido was stable enough to be isolated as a single crystal in acetonitrile.

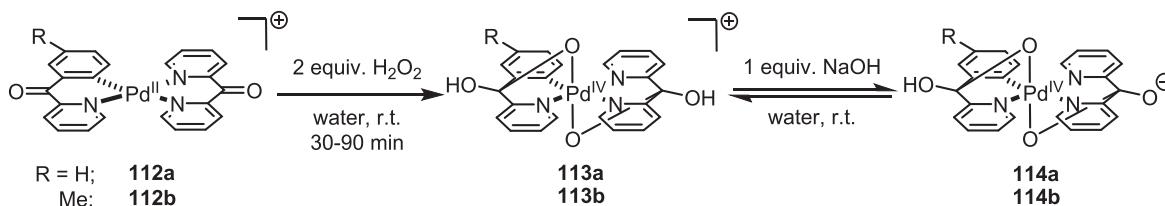


Fig. 49 Pd^{IV} complexes supported by facially chelating NNO and NCO ligands.

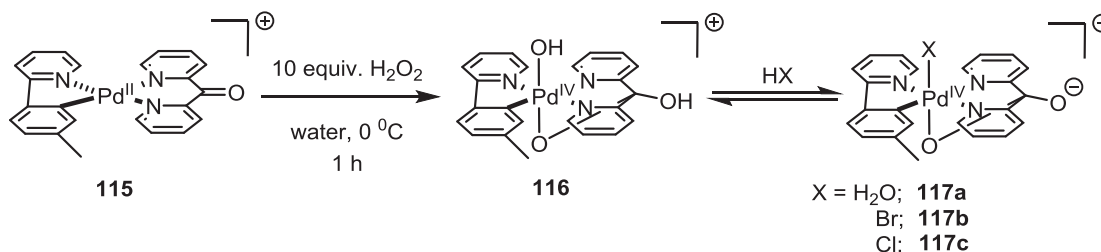


Fig. 50 Pd^{IV} complexes supported by a facially chelating NNO ligand.

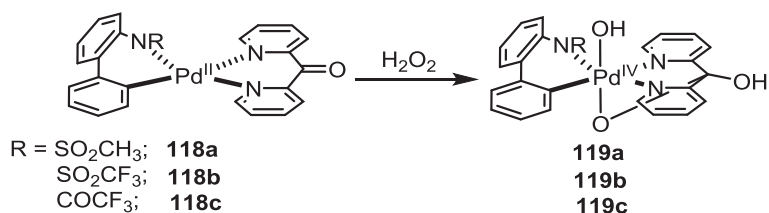


Fig. 51 Pd^{IV} complexes supported by a dipyritylketone ligand.

6.10.3.3.3 Pd^{IV} complexes stabilized by di(pyridin-2-yl)methane ligands

Di-2-pyridylmethanesulfonate had been previously employed by the Vedernikov group to explore high valent platinum-dioxygen chemistry. Complex **121** was produced by reacting the Pd^{II}Me(OH) precursor **120** with MeI (Fig. 52).⁶⁹ While the complex was too unstable to be crystallographically characterized, it was characterized by NMR spectroscopy. Selective NOE experiments were carried and showed an interaction between the axial methyl ligand (2.91 ppm) and both *o*-C-H protons of the ligand pyridine rings. An interaction between the axial and equatorial (2.51 ppm) methyl ligands was also observed. The relative instability of the complex can be attributed to the weakly donating nature of the sulfonate ligand.

Sanford and co-workers introduced two related facially chelating tridentate ligands with NNN and NNC donor atoms to stabilize Pd^{IV} complexes (Fig. 53).⁷⁰ They reported the isolation and crystallographic characterization of a host of complexes **122** and **123** with different *trans*-axial ligands, which were able to stabilize Pd^{IV} complexes against reductive elimination pathways. The NNC ligand-based complexes showed facile C–H activation at Pd^{IV} and ligand substitution processes, where both anionic and neutral complexes were exchanged with halides and triflates.

6.10.3.3.4 Pd^{IV} complexes stabilized by the Kläui ligand

Pd^{IV} complexes with O-donor chelating ligands are less common than C- or N-donors. Leung and co-workers reported the synthesis and characterization of Pd^{IV} complexes **125** supported by Kläui's tripodal ligand (Fig. 54).⁷¹ The complexes were synthesized by treating the Pd^{II} precursors with PhICl₂. The crystal structure of **125** revealed differences in Pd–O bond lengths (2.155(3) Å, 2.104(3) Å, and 2.024(3) Å) as expected from the differing *trans*-influence of the opposing ligands (Ph[−] > PPh₃ > Cl[−]). Complex **127** showed similar trends in bond lengths. It is interesting to note that the Pd^{IV} center is stereogenic in these complexes, and the complexes were isolated as racemic mixtures.

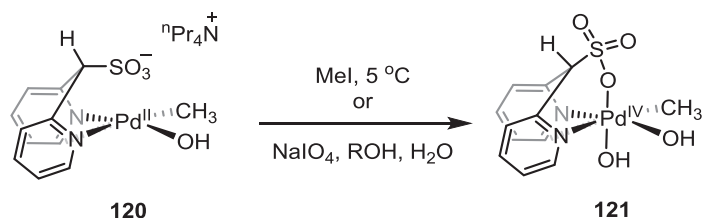


Fig. 52 A Pd^{IV} complex stabilized by a di-2-pyridylmethanesulfonate ligand.

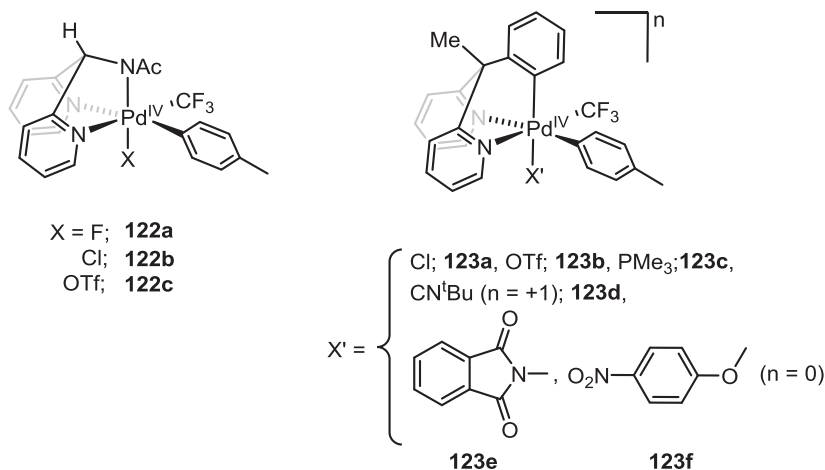


Fig. 53 Pd^{IV} complexes stabilized by facially chelating NNN and NNC ligands.

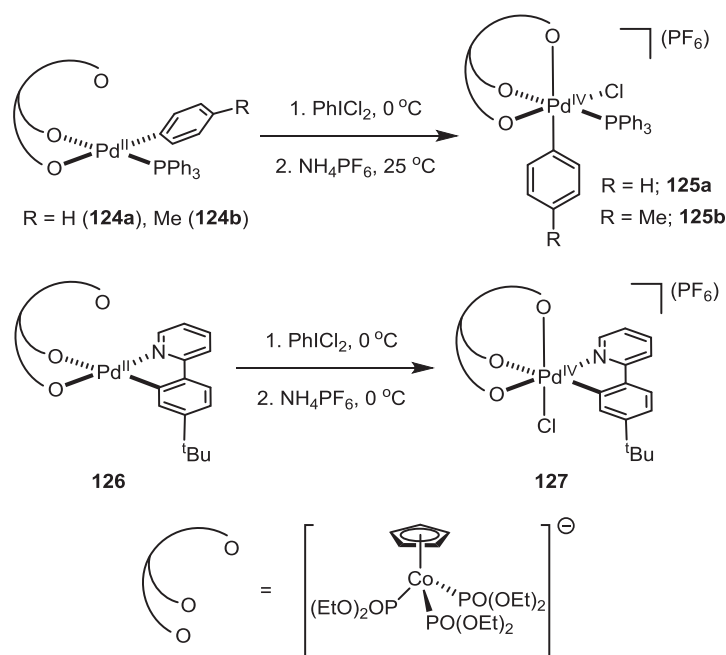


Fig. 54 Pd^{IV} complexes stabilized by the Kläui tripodal ligand.

6.10.3.4 Pd^{IV} Complexes Stabilized by Tridentate Planar Ligands

The Canty group studied the formation of alkynyl palladium and platinum complexes supported by diphosphine and pincer ligands. While the platinum complexes were fairly stable and diffraction quality crystals could be obtained, the palladium analogs could only be characterized by low-temperature NMR experiments.⁷² The structure of complex **129** was established by comparing the spectral features obtained from the reaction of the analogous platinum complex (Fig. 55). For the NCN pincer system, (NCN)Pd^{II}(CO₂Ph) was reacted with phenyl[(trimethylsilyl)ethynyl]iodonium triflate at $-80\text{ }^\circ\text{C}$ for a week. The resulting spectrum was consistent with the complexes **131** and **132** shown below by comparing the resonances and proton integrations with the Pt complex. The authors, however, could not make a confident prediction of the relative orientation of the triflate and benzoate ligands from the NMR spectra alone.

6.10.3.4.1 Pd^{IV} complexes stabilized by pincer ligands

Szabo and co-workers utilized a tridentate NCN pincer ligand to explore the reactivity of high-valent Pd complexes (Fig. 56).⁷³ They proposed the intermediacy of complex **134** in a C-H acetoxylation reaction. On reacting the Pd^{II} complex **133** with PhI(OAc)₂, they observed changes in the NMR spectrum, which were consistent with a Pd^{IV} complex. The shifts and splitting patterns indicated the formation of an octahedral complex with a reduced C_s symmetry and were consistent with the NMR spectra of similar complexes by Canty and van Koten.

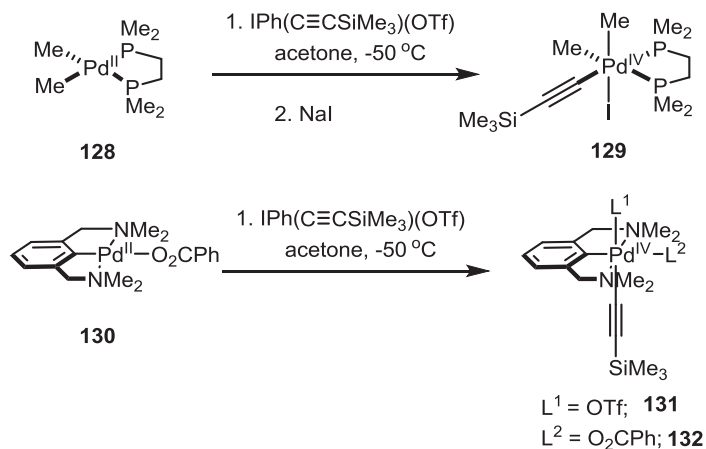


Fig. 55 Synthesis of alkynyl Pd^{IV} complexes supported by a NCN pincer ligand.

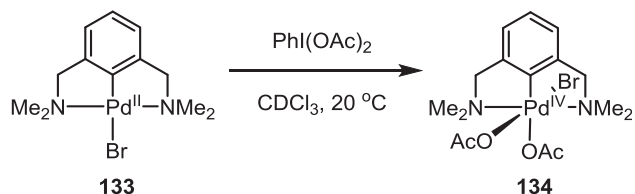


Fig. 56 Synthesis of an NCN pincer Pd^{IV} complex using PhI(OAc)₂.

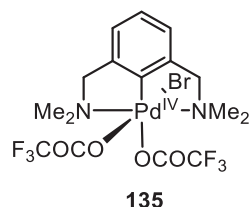


Fig. 57 A Pd^{IV}-trifluoroacetate complex supported by an NCN pincer ligand.

In related work, Szabo and co-workers proposed the involvement of high-valent palladium intermediates in C–H borylation chemistry (Fig. 57).⁷⁴ They proposed intermediate 135 in the catalytic cycle, which undergoes transmetalation with TFA-Bpin to continue further in the cycle and ultimately yield C–H borylated olefins. The intermediate was well characterized by NMR and showed the characteristics of a transient Pd^{IV} complex.

Though pincer complexes have been widely used to stabilize Pd^{IV} complexes due to their exceptional chelating ability, examples of isolated crystal structures had been limited to scorpionate or bis-chelating bipyridyl motifs. In 2010, the Bautista group isolated and characterized Pd^{IV} complexes supported by ONC pincer ligands (Fig. 58). They formed the Pd^{IV} complex 138 by the oxidative addition of halogens to the Pd^{II} complex 136.⁷⁵ It is interesting to note that this complex could be isolated, whereas the previous ones supported by pincer ligands were only characterized by NMR. This could possibly be due to the fact that the weakly donating OMe group is *trans* to the σ -C_{sp}3 carbon. This attenuates the *trans* effect of the σ -C_{sp}3 carbon, which can lead to facile decomposition pathways.

Extending their work with the ONC type pincer ligands, Bautista and co-workers utilized the conformational flexibility of one of the arms of the ligand to oxidatively add an aryl halide and isolate the corresponding Pd^{IV} complex.⁷⁵ They hypothesized that the proximity of the iodide to the Pd^{II} center in intermediate would allow facile oxidative addition, which would be assisted by dechelation of the OMe group (Fig. 59).^{76–78} The stability of the complex is increased by two chelating palladacycles, which counteract

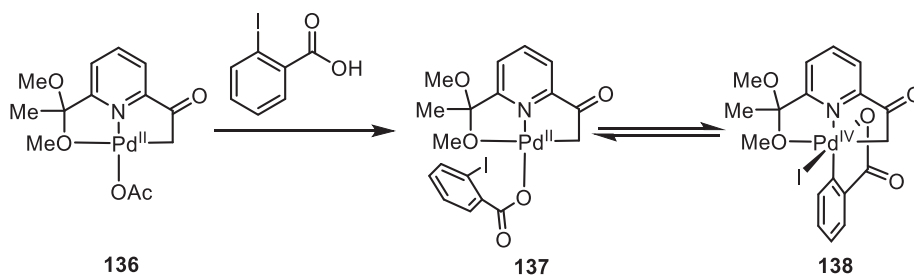


Fig. 58 The first crystallographically characterized ONC pincer-supported Pd^{IV} complex.

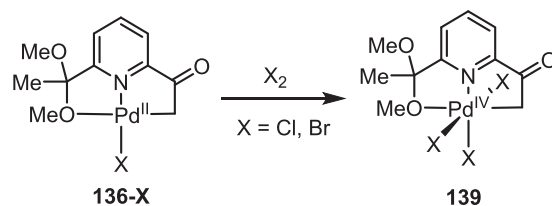


Fig. 59 ONC pincer-supported trihalo Pd^{IV} complexes.

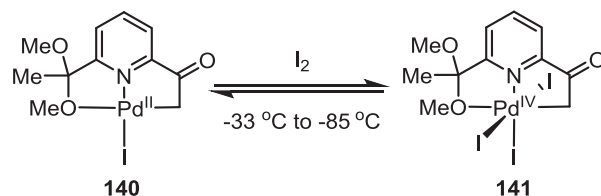


Fig. 60 ONC pincer-supported triiodo Pd^{IV} complex.

possible dissociation routes owing to the strong *trans*-influence of the σ -aryl Pd–C bonds. Moreover, they were able to react the Pd^{II} precursor 136-X with halogens to generate the Pd^{IV} complexes 139, which were isolated and characterized by X-ray crystallography,

To complete the series of the previously reported the synthesis of the tri- chloro and bromo Pd^{IV} complexes with the ONC pincer ligand, the tri-iodo complex 141 was successfully synthesized by the oxidative addition of I₂ with the Pd^{II} precursor in a later report (Fig. 60). The notable structural feature of this complex is the significantly longer Pd–N bond length of 2.045(3) Å relative to the Pd–N bond lengths of its chloro and bromo congeners of 2.0207(15) Å and 2.0058(15) Å, respectively, which falls in line with the *trans*-influence ordering of the halide ligands: I[−] > Br[−] > Cl[−].^{76–78}

The Gaunt group had previously posited the existence of a Pd^{IV} intermediate in C–H arylation chemistry involving the reaction of a five-membered ring aminoalkyl palladacycle and 2-iodobenzoic acid. They successfully isolated the intermediate in 2020 by making use of the chelate effect of a pincer ligand containing anionic OCO donors by reacting the aminoalkyl Pd^{II} precursor with a pyridine 2,6-dicarboxylate species.⁷⁹ Complex 142 has the two carbon ligands bind *cis* to one another, avoiding the potential destabilization from the *trans* effect of these groups that are often seen in other complexes (Fig. 61). The *trans* effect is clearly seen for the pyridine located *trans* to the sp³–C of the palladacycle, showing an elongated C–N bond length (2.231(8) Å) and dissociating on exposure to vacuum. The related complex 143 was isolated using the same OCO pincer ligand, starting from a cyclopalladated oxime precursor rather than an aminoalkyl group. The oxime binds more strongly to the Pd^{IV} center, and the Pd–N bond length for the pyridine is slightly shorter (2.120(8) Å).

6.10.3.4.2 Pd^{IV} complexes stabilized by terpyridyl ligands

The Ritter group developed a method for electrophilic aromatic C–H fluorination, and the Pd^{IV} complex 145 was isolated as a part of their mechanistic investigations (Fig. 62).⁸⁰ This complex contains a more electron-rich phenanthroline ligand in the active catalyst (2-Cl-phenanthroline), which made it more stable. The authors invoked an uncommon electrophilic F⁺ transfer mechanism from the species 145, which is reminiscent of the group transfer reactivity of metal-oxo or metal-nitrenoid complexes.

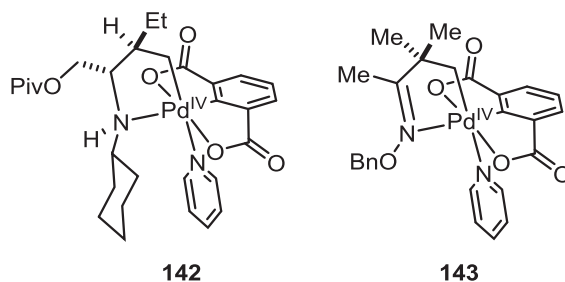


Fig. 61 Aminoalkyl-Pd^{IV} complexes supported by OCO pincer ligands.

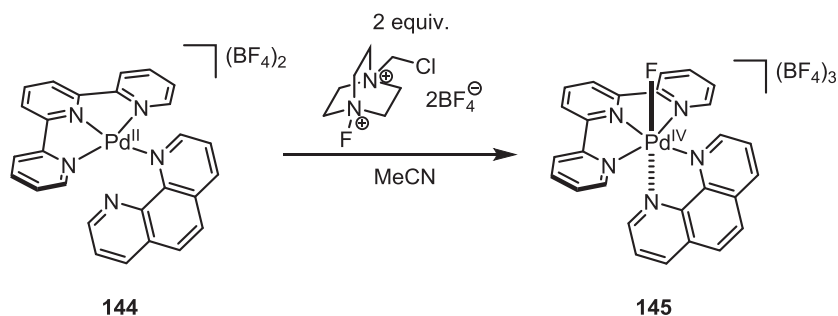


Fig. 62 A Pd^{IV} complex supported by terpyridine and phenanthroline.

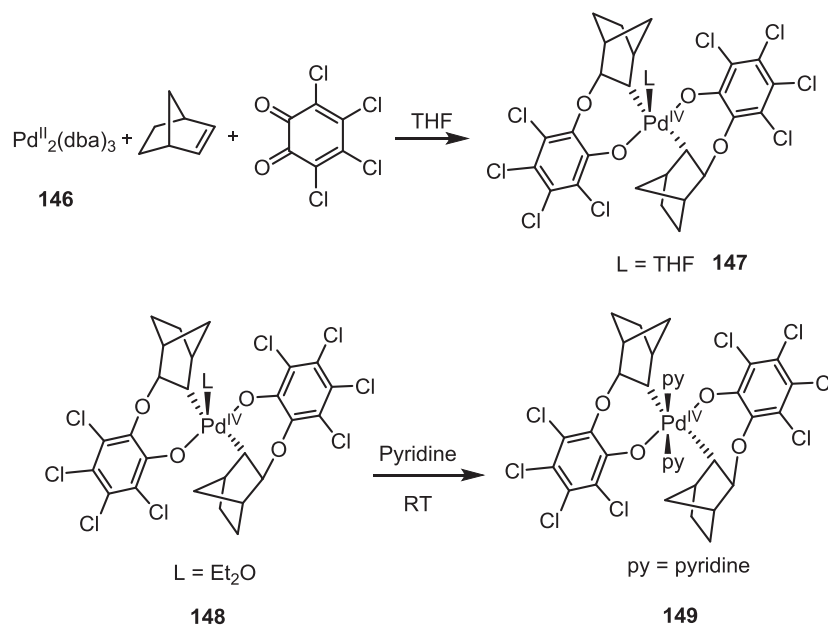


Fig. 63 C_2 -symmetric spirocyclic Pd^{IV} complexes with norbornene ligands.

6.10.3.5 Pd^{IV} Complexes Stabilized by Other Ligand Systems

In 2002, Itoh and coworkers synthesized a C_2 -symmetric spirocyclic Pd^{IV} complexes 147 and 148 by a tandem oxidative cyclization between *o*-chloranil and norbornene with a Pd^0 precursor (Fig. 63).⁸¹ This reaction is remarkable since the previous syntheses of Pd^{IV} complexes relied on bidentate or tridentate ligands to prevent the formation of pentacoordinate Pd intermediates that undergo rapid reductive elimination. Even though quinones are known to be redox-active, the crystal structure parameters for 147 and the absence of C=O stretches in the molecule indicated that there was no residual benzoquinone character in the *o*-chloranil ligands. The complex is trigonal bipyramidal, with the oxygen atoms from *o*-chloranil occupying the axial positions and the carbon atoms from the norbornane occupying two of the equatorial positions. The axial position is occupied by a THF molecule in 147 or by a Et_2O molecule on 148, both of which are labile to ligand substitution. In fact, the two tetrachlorophenyl rings are turned away from the coordination sites in the same direction as norbornane, which makes the complex flexible in terms of coordination number. When Et_2O was substituted with pyridine, a six-coordinate Pd^{IV} complex 149 was formed, with the two pyridines occupying the two axial positions.

The same group found that using benzonorbornadiene as the olefin also produced a similar palladacyclic complex 150, which has a greater stability compared to 147 in solution.⁸² Additional Pd^{IV} complexes were isolated, with a THF molecule, in 151, and a pyridine, in 152, occupying the axial position (Fig. 64). The thermolysis of 152 leads thermal decomposition to furnish benzonorbornadiene. The decomposition was retarded by adding five equivalents of pyridine, which hampers the formation of the reactive four-coordinate intermediate.

The Weseman group examined the efficacy of stanna-*closo*-dodecaborate as a ligand for Ni^{IV} , Pd^{IV} , and Pt^{IV} centers.⁸³ The Pd complex 152 was synthesized from a Pd^{IV} precursor salt and the stannaborate ligand, exhibiting near-perfect octahedral coordination by the six tin ligands (Fig. 65). The authors noted that the Pd–Sn distances were considerably shorter than the reported intermetallic stannides (2.78–2.84 Å in PdSn_2 , PdSn_3 , and PdSn_4). The compounds were fully characterized in solution by multinuclear NMR spectroscopy.

The Daugulis group pioneered the use of the 8-aminoquinoline motif for directed C–H bond activation chemistry. The reaction of a cyclometalated 8-aminoquinoline pivalamide Pd^{II} complex with bromine at -78°C afforded complex 156, which was characterized by X-ray crystallography (Fig. 66).⁸⁴ Because dissociation of one ligand is often invoked in decomposition pathways, the authors attributed the stability of the complex to the strongly binding $^1\text{BuCN}$ ligand, in addition to strong chelation by the pivalamide.

The Fedin group explored the structural and redox properties of a Pd^{IV} -cyclam complex 157 within the cavity of cucurbit[8]uril.⁸⁵ Such inclusion compounds often display unique properties relative to the free complex and are of interest in drug delivery. The $[\text{Pd}^{\text{IV}}(\text{cyclam})\text{Cl}_2]^{2+}$ complex was prepared by the oxidation of the $\text{Pd}^{\text{II}}(\text{cyclam})$ precursor inside the cavity of the cucurbit[8]uril using NO_2 in a concentrated HCl solution (Fig. 67).

The Kraft group made use of a bis-NHC scaffold developed by Strassner and co-workers to explore stoichiometric chlorination reactions involving alkenes, alkynes, as well as C–H bond activation.⁸⁶ Though these ligands are similar to the pyridinophanes in their coordination geometry, this is one of the few reported examples of an NHC ligand being used to stabilize Pd^{IV} centers (Fig. 68). The complexes featured significantly longer equatorial Pd–Cl bonds, relative to the axial Pd–Cl bonds, underlining

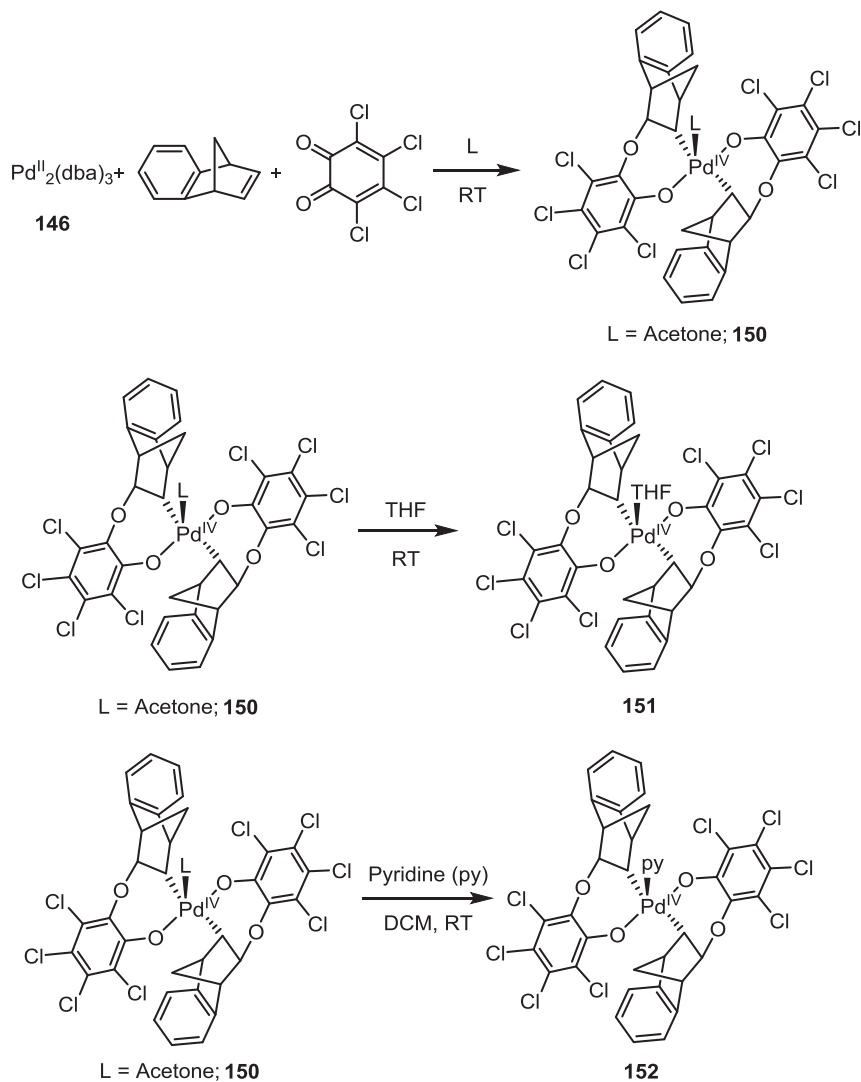
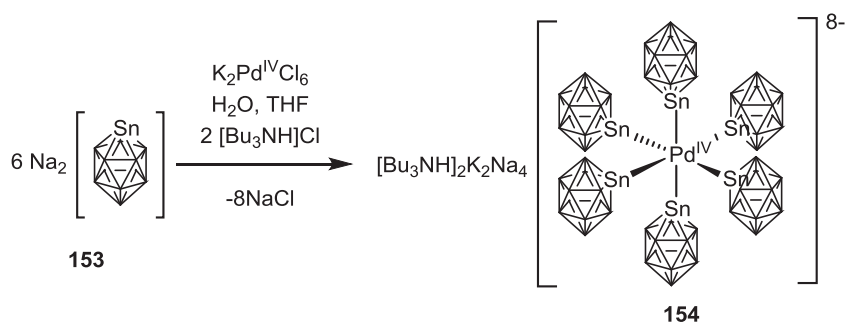


Fig. 64 C_2 -symmetric spirocyclic Pd^{IV} complexes with benzenorbornene ligands.



All vertices of the dodecahedron are BH units

Fig. 65 A Pd^{IV} complex supported by stanna-*closo*-dodecaborate ligands.

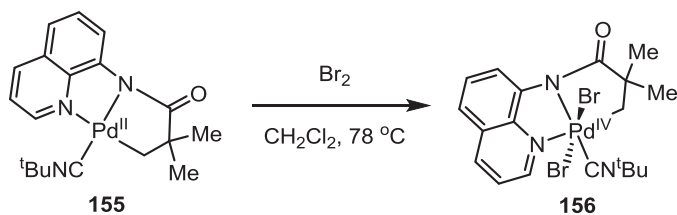


Fig. 66 A Pd^{IV} complex supported by 8-aminoquinoline pivalamide.

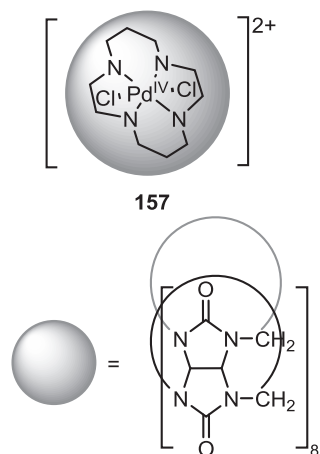


Fig. 67 A Pd^{IV}-dichloro complex supported by a cyclam ligand inside the cavity of cucurbit[8]uril.

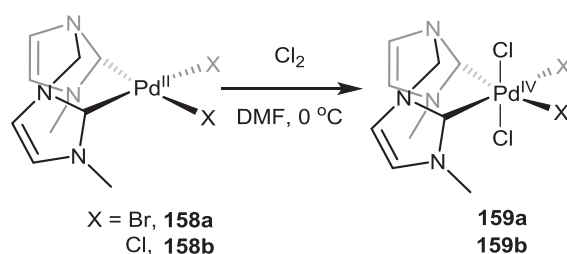


Fig. 68 Bis-NHC-stabilized Pd^{IV} tetrachloro complexes.

the strong *trans* influence of the NHC ligands. Pd–C_{carbene} bonds experienced a lengthening of 0.046 and 0.049 Å with respect to the Pd^{II} precursor. This was explained by a diminished donation of metal-based d-electrons into the π-orbitals based on the NHC ligand. Interestingly, the authors noted a hydrogen bonding interaction between the protons of the NHC ligand scaffold and axial chloride anions, which led to the formation of supramolecular adducts. These interactions were also found to accelerate chloronium (Cl⁺) ion transfers in the chlorination of unsaturated bonds by these complexes.

In 2014, Lash and co-workers reported an unusual Pd^{IV} complex **161**, which was stabilized as a sandwich complex in a dicarbaporphyrin ligand framework.⁸⁷ The reaction of Pd(OAc)₂ with the dicarbaporphyrin ligand **160** resulted in a trinuclear complex **161**, where two square planar porphyrinoid macrocycles contained Pd^{II} ions, while the coordination mode of Pd^{IV} is unique as it involves two subunits and the *meso* carbon of the porphyrin rings (Fig. 69). In effect, the dianionic ligands contribute to 6 π-electrons each, resulting in a stable 18 e⁻ system. The short average Pd–C bond (2.338 Å) indicates a fairly strong bond. This was the first report of a porphyrinoid ligand with a *meso*-carbon-bound Pd involved in a hapticity greater than η².

Lampeka, Arion, and co-workers isolated a Pd^{IV} dichloro complex **162**, formed by oxidizing a Pd^{II} precursor with potassium peroxodisulfate in the presence of chloride ions (Fig. 70).⁸⁸ The ligand is a rare example of an amine-amide donor set within a markedly skewed oxamide chelate ring. These complexes were fairly stable in aqueous solutions to be used for cytotoxicity studies.

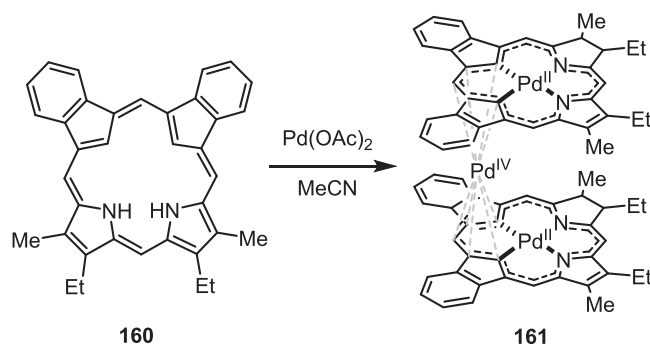


Fig. 69 A sandwich Pd^{IV} complex stabilized by a dicarbaporphyrin ligand.

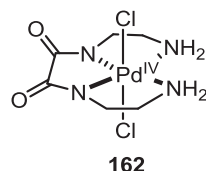


Fig. 70 A Pd^{IV} dichloro complex featuring amine-amide donor atoms.

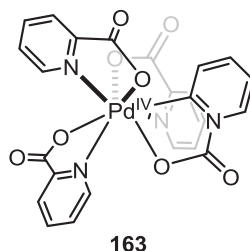


Fig. 71 A distorted dodecahedral Pd^{IV} complex stabilized by pyridine-2-carboxylate ligands.

In 2009, an unusual distorted dodecahedral Pd^{IV} complex, **163**, was isolated by Kim and Ha.⁸⁹ The Pd^{IV} center, which usually prefers an octahedral coordination environment, was 8-coordinate and supported by four pyridine-2-carboxylate ligands, which showed dodecahedral coordination in the solid-state structure (Fig. 71). The adjacent pyridine rings were reported to have π - π interactions between them. Notably, this is one of the few reported structures not featuring a Pd–C bond.

6.10.4 Summary and Outlook

In summary, we have provided a comprehensive overview of the structurally characterized Pd^{III} and Pd^{IV} complexes that have been isolated and characterized by various groups since 2003. This chapter showcases the first reported organometallic dinuclear Pd^{III} complexes, published in 2006, and the first mononuclear organometallic Pd^{III} complexes, published in 2010. Brief synthesis methodologies, structural properties, and the reactivity of these organometallic complexes have also been discussed. Furthermore, we also included various examples of dinuclear and molecular 1D chain bearing Pd^{III} backbones that have been well-characterized using X-ray crystallography and traditional spectroscopic techniques.

We have also discussed the strategies employed behind the isolation of Pd^{IV} complexes, which have been proposed as intermediates in various organic transformations. A range of ligand frameworks have been successfully employed to arrest the reductive elimination reactions which usually limit the stability of these Pd^{IV} complexes. Overall, the judicious choice of chelating ligands and their steric and electronic properties seems to be paramount for the stabilization of such high-valent Pd complexes. Moreover, we expect that the structural insights gained from the detailed characterization of these intermediates will lead to the development of more specific uses of high-valent Pd species in catalysis and other applications.

References

- Chen, X.; Engle, K. M.; Wang, D.-H.; Yu, J.-Q. *Angew. Chem., Int. Ed.* **2009**, *48*, 5094–5115.
- Hickman, A. J.; Sanford, M. S. *Nature* **2012**, *484*, 177–185.
- Mirica, L. M.; Khusnutdinova, J. R. *Coord. Chem. Rev.* **2013**, 299–314.
- Topczewski, J. J.; Sanford, M. S. *Chem. Sci.* **2015**, *6*, 70–76.
- Powers, D. C.; Ritter, T. *Top. Organomet. Chem.* **2011**, *35*, 129–156.
- Sehna, P.; Taylor, R. J. K.; Fairlamb, I. J. S. *Chem. Rev.* **2010**, *110*, 824–889.
- Xu, L.-M.; Li, B.-J.; Yang, Z.; Shi, Z.-J. *Chem. Soc. Rev.* **2010**, *39*, 712–733.
- Lyons, T. W.; Sanford, M. S. *Chem. Rev.* **2010**, *110*, 1147–1169.
- Khusnutdinova, J. R.; Rath, N. P.; Mirica, L. M. *J. Am. Chem. Soc.* **2010**, *132*, 7303–7305.
- Khusnutdinova, J. R.; Rath, N. P.; Mirica, L. M. *J. Am. Chem. Soc.* **2012**, *134*, 2414–2422.
- Tang, F. Z.; Park, S. V.; Rath, N. P.; Mirica, L. M. *Dalton Trans.* **2018**, *47*, 1151–1158.
- Khusnutdinova, J. R.; Mirica, L. M. *Organometallic Pd(III) Complexes in C-C and C-Heteroatom Bond Formation Reactions*. In *C-H and C-X Bond Functionalization: Transition Metal Mediation*; Ribas, X., Ed.; Royal Society of Chemistry, 2013; pp 122–158.
- Tang, F.; Ou, F.; Khusnutdinova, J. R.; Rath, N. P.; Mirica, L. M. *Dalton Trans.* **2012**, *41*, 14046–14050.
- Schultz, J. W.; Rath, N. P.; Mirica, L. M. *Inorg. Chem.* **2020**, *59*, 11782–11792.
- Khusnutdinova, J. R.; Rath, N. P.; Mirica, L. M. *Inorg. Chem.* **2014**, *53*, 13112–13129.
- Ruhs, N. P.; Khusnutdinova, J.; Rath, N. P.; Mirica, L. M. *Organometallics* **2019**, *38*, 3834–3843.
- Niu, J.-L.; Hao, X.-Q.; Gong, J.-F.; Song, M.-P. *Dalton Trans.* **2011**, *40*, 5135–5150.
- Stephen, E.; Blake, A. J.; Carter, E.; Collison, D.; Davies, E. S.; Edge, R.; Lewis, W.; Murphy, D. M.; Wilson, C.; Gould, R. O.; Holder, A. J.; McMaster, J.; Schröder, M. *Inorg. Chem.* **2012**, *51*, 1450–1461.

19. Mazzotti, A. R.; Campbell, M. G.; Tang, P.; Murphy, J. M.; Ritter, T. *J. Am. Chem. Soc.* **2013**, *135*, 14012–14015.
20. Berry, J. F.; Bill, E.; Bothe, E.; Cotton, F. A.; Dalal, N. S.; Ibragimov, S. A.; Kaur, N.; Liu, C. Y.; Murillo, C. A.; Nellutta, S.; North, J. M.; Villagran, D. *J. Am. Chem. Soc.* **2007**, *129*, 1393–1401.
21. Cotton, F. A.; Matusz, M.; Poli, R.; Feng, X. *J. Am. Chem. Soc.* **1988**, *110*, 1144.
22. Cotton, F. A.; Matusz, M.; Poli, R. *Inorg. Chem.* **1987**, *26*, 1472–1474.
23. Cotton, F. A.; Koshevoy, I. O.; Lahuerta, P.; Murillo, C. A.; Sanau, M.; Ubeda, M. A.; Zhao, Q. *J. Am. Chem. Soc.* **2006**, *128*, 13674–13675.
24. Penno, D.; Lillo, V.; Koshevoy, I. O.; Sanau, M.; Ubeda, M. A.; Lahuerta, P.; Fernandez, E. *Chem. – Eur. J.* **2008**, *14*, 10648–10655.
25. Penno, D.; Estevan, F.; Fernandez, E.; Hirva, P.; Lahuerta, P.; Sanau, M.; Ubeda, M. A. *Organometallics* **2011**, *30*, 2083–2094.
26. Estevan, F.; Hirva, P.; Ofori, A.; Sanaú, M.; Špec, T.; Ubeda, M. *Inorg. Chem.* **2016**, *55*, 2101–2113.
27. Powers, D. C.; Geibel, M. A. L.; Klein, J.; Ritter, T. *J. Am. Chem. Soc.* **2009**, *131*, 17050–17051.
28. Powers, D. C.; Ritter, T. *Nat. Chem.* **2009**, *1*, 302–309.
29. Berry, J. F.; Cotton, F. A.; Ibragimov, S. A.; Murillo, C. A.; Wang, X. *Inorg. Chem.* **2005**, *44*, 6129–6137.
30. Ye, Y.; Ball, N. D.; Kampf, J. W.; Sanford, M. S. *J. Am. Chem. Soc.* **2010**, *132*, 14682–14687.
31. Powers, D. C.; Lee, E.; Ariafard, A.; Sanford, M. S.; Yates, B. F.; Canty, A. J.; Ritter, T. *J. Am. Chem. Soc.* **2012**, *134*, 12002–12009.
32. Powers, D. C.; Benitez, D.; Ktatchouk, E.; Goddard, W. A.; Ritter, T. *J. Am. Chem. Soc.* **2010**, *132*, 14092–14103.
33. Bonney, K. J.; Schoenebeck, F. *Chem. Soc. Rev.* **2014**, *43*, 6609–6638.
34. Nielsen, M. C.; Lyngvi, E.; Schoenebeck, F. *J. Am. Chem. Soc.* **2013**, *135*, 1978–1985.
35. Trinquier, G.; Hoffmann, R. *Organometallics* **1984**, *3*, 370–380.
36. Khusnutdinova, J. R.; Rath, N. P.; Mirica, L. M. *Angew. Chem., Int. Ed.* **2011**, *50*, 5532–5536.
37. Takaishi, S.; Takamura, M.; Kajiwara, T.; Miyasaka, H.; Yamashita, M.; Lwata, M.; Matsuzaki, H.; Okamoto, H.; Tanaka, H.; Kuroda, S.; Nishikawa, H.; Oshio, H.; Kato, K.; Takata, M. *J. Am. Chem. Soc.* **2008**, *130*, 12080–12084.
38. Yamashita, M.; Takaishi, S. *Chem. Comm.* **2010**, *46*, 4438–4448.
39. Kumagai, S.; Takaishi, S.; Breedlove, B. K.; Okamoto, H.; Tanaka, H.; Kuroda, S.-I.; Yamashita, M. *Chem. Comm.* **2014**, *50*, 8382–8384.
40. Eitel, S. H.; Bauer, M.; Schweinfurth, D.; Deibel, N.; Sarkar, B.; Kelm, H.; Krüger, H.-J.; Frey, W.; Peters, R. *J. Am. Chem. Soc.* **2012**, *134*, 4683–4693.
41. Kumagai, S.; Takaishi, S.; Gao, M.; Iguchi, H.; Breedlove, B. K.; Yamashita, M. *Inorg. Chem.* **2018**, *57*, 3775–3781.
42. Hisamitsu, A.; Daisuke, K.; Shinya, T.; Takashi, K.; Hitoshi, M.; Ken-ichi, S.; Masahiro, Y.; Hideo, K.; Hiroshi, O. *Bull. Chem. Soc. Jpn.* **2007**, *80*, 189–191.
43. Wong, W. K.; Liang, H. Z.; Yung, M. Y.; Guo, H. P.; Yung, K. F.; Wong, W. T.; Edwards, P. G. *Inorg. Chem. Commun.* **2004**, *7*, 737–740.
44. Canty, A. J.; Hettling, M. J. G.; Patel, J.; Pfeffer, R.; Skelton, B. W.; White, A. H. *Inorg. Chim. Acta* **2002**, *338*, 94–98.
45. Canty, A. J.; Patel, J.; Rodemann, T.; Ryan, J. H.; Skelton, B. W.; White, A. H. *Organometallics* **2004**, *23*, 3466–3473.
46. Dick, A. R.; Kampf, J. W.; Sanford, M. S. *J. Am. Chem. Soc.* **2005**, *127*, 12790–12791.
47. Whitfield, S. R.; Sanford, M. S. *J. Am. Chem. Soc.* **2007**, *129*, 15142–15143.
48. Guo, R. Y.; Portscher, J. L.; Day, V. W.; Malinakova, H. C. *Organometallics* **2007**, *26*, 3874–3883.
49. Furuya, T.; Ritter, T. *J. Am. Chem. Soc.* **2008**, *130*, 10060–10061.
50. Ball, N. D.; Sanford, M. S. *J. Am. Chem. Soc.* **2009**, *131*, 3796–3799.
51. Racowski, J. M.; Gary, J. B.; Sanford, M. S. *Angew. Chem., Int. Ed.* **2012**, *51*, 3414–3417.
52. Pendleton, I. M.; Perez-Temprano, M. H.; Sanford, M. S.; Zimmerman, P. M. *J. Am. Chem. Soc.* **2016**, *138*, 6049–6060.
53. Zhao, X. D.; Dong, V. M. *Angew. Chem., Int. Ed.* **2011**, *50*, 932–934.
54. Ball, N. D.; Gary, J. B.; Ye, Y.; Sanford, M. S. *J. Am. Chem. Soc.* **2011**, *133*, 7577–7584.
55. Racowski, J. M.; Ball, N. D.; Sanford, M. S. *J. Am. Chem. Soc.* **2011**, *133*, 18022–18025.
56. Amatore, C.; Catellani, M.; Deledda, S.; Jutand, A.; Motti, E. *Organometallics* **2008**, *27*, 4549–4554.
57. Arnold, P. L.; Sanford, M. S.; Pearson, S. M. *J. Am. Chem. Soc.* **2009**, *131*, 13912–13913.
58. Khusnutdinova, J. R.; Qu, F.; Zhang, Y.; Rath, N. P.; Mirica, L. M. *Organometallics* **2012**, *31*, 4627–4630.
59. Qu, F.; Khusnutdinova, J. R.; Rath, N. P.; Mirica, L. M. *Chem. Comm.* **2014**, *50*, 3036–3039.
60. Luo, J.; Rath, N. P.; Mirica, L. M. *Organometallics* **2013**, *31*, 3343–3353.
61. Campora, J.; Palma, P.; del Rio, D.; Carmona, E.; Graiff, C.; Tiripicchio, A. *Organometallics* **2003**, *22*, 3345–3347.
62. Campora, J.; Palma, P.; del Rio, D.; Lopez, J. A.; Valerga, P. *Chem. Comm.* **2004**, 1490–1491.
63. Campora, J.; Palma, P.; del Rio, D.; Lopez, J. A.; Alvarez, E.; Connelly, N. G. *Organometallics* **2005**, *24*, 3624–3628.
64. Camasso, N. M.; Canty, A. J.; Ariafard, A.; Sanford, M. S. *Organometallics* **2017**, *36*, 4382–4393.
65. Daryanavard, M.; Armstrong, D.; Lough, A. J.; Fekl, U. *Dalton Trans.* **2017**, *46*, 4004–4008.
66. Maleckis, A.; Kampf, J. W.; Sanford, M. S. *J. Am. Chem. Soc.* **2013**, *135*, 6618–6625.
67. Oloo, W.; Zavalij, P. Y.; Zhang, J.; Khaskin, E.; Vedernikov, A. N. *J. Am. Chem. Soc.* **2010**, *132*, 14400–14402.
68. Abada, E.; Zavalij, P. Y.; Vedernikov, A. N. *J. Am. Chem. Soc.* **2017**, *139*, 643–646.
69. Sberegaeva, A. V.; Zavalij, P. Y.; Vedernikov, A. N. *J. Am. Chem. Soc.* **2016**, *138*, 1446–1455.
70. Maleckis, A.; Sanford, M. S. *Organometallics* **2011**, *30*, 6617–6627.
71. So, Y.-M.; Au-Yeung, K.-C.; Sung, H. H.-Y.; Williams, I. D.; Leung, W.-H. *Eur. J. Inorg. Chem.* **2017**, *2017*, 2928–2935.
72. Canty, A. J.; Rodemann, T.; Skelton, B. W.; White, A. H. *Organometallics* **2006**, *25*, 3996–4001.
73. Pilarski, L. T.; Selander, N.; Bose, D.; Szabo, K. J. *Org. Lett.* **2009**, *11*, 5518–5521.
74. Selander, N.; Willy, B.; Szabó, K. J. *Angew. Chem., Int. Ed.* **2010**, *49*, 4051–4053.
75. Vicente, J.; Arcas, A.; Juliá-Hernández, F.; Bautista, D. *Angew. Chem., Int. Ed.* **2011**, *50*, 6896–6899.
76. Martínez-Martínez, A.-J.; Chicote, M.-T.; Bautista, D.; Vicente, J. *Organometallics* **2012**, *31*, 3711–3719.
77. Vicente, J.; Arcas, A.; Juliá-Hernández, F.; Bautista, D. *Chem. Comm.* **2010**, *46*, 7253–7255.
78. Vicente, J.; Arcas, A.; Juliá-Hernández, F.; Bautista, D. *Inorg. Chem.* **2011**, *50*, 5339–5341.
79. Whitehurst, W. G.; Gaunt, M. J. *J. Am. Chem. Soc.* **2020**, *142*, 14169–14177.
80. Yamamoto, K.; Li, J.; Garber, J. A. O.; Rolfes, J. D.; Boursalian, G. B.; Borghs, J. C.; Genicot, C.; Jacq, J.; van Gestel, M.; Neese, F.; Ritter, T. *Nature* **2018**, *554*, 511–514.
81. Yamamoto, Y.; Ohno, T.; Itoh, K. *Angew. Chem., Int. Ed.* **2002**, *41*, 3662–3665.
82. Yamamoto, Y.; Kuwabara, S.; Matsuo, S.; Ohno, T.; Nishiyama, H.; Itoh, K. *Organometallics* **2004**, *23*, 3898–3906.
83. Kirchmann, M.; Eichele, K.; Schappacher, F. M.; Pöttgen, R.; Wesemann, L. *Angew. Chem., Int. Ed.* **2008**, *47*, 963–966.
84. Shabashov, D.; Daugulis, O. *J. Am. Chem. Soc.* **2010**, *132*, 3965–3972.
85. Mitkina, T. V.; Naumov, D. Y.; Gerasko, O. A.; Fedin, V. P. *Inorg. Chim. Acta* **2010**, *363*, 4387–4391.
86. McCall, A. S.; Wang, H.; Desper, J. M.; Kraft, S. *J. Am. Chem. Soc.* **2011**, *133*, 1832–1848.
87. AbuSalim, D. I.; Ferrence, G. M.; Lash, T. D. *J. Am. Chem. Soc.* **2014**, *136*, 6763–6772.
88. Gavriš, S. P.; Lampeka, Y. D.; Babak, M. V.; Arion, V. B. *Inorg. Chem.* **2018**, *57*, 1288–1297.
89. Kim, N.-H.; Ha, K. *Acta Cryst. Sec. E* **2009**, *65*, m1274.